Euscorpius

Occasional Publications in Scorpiology

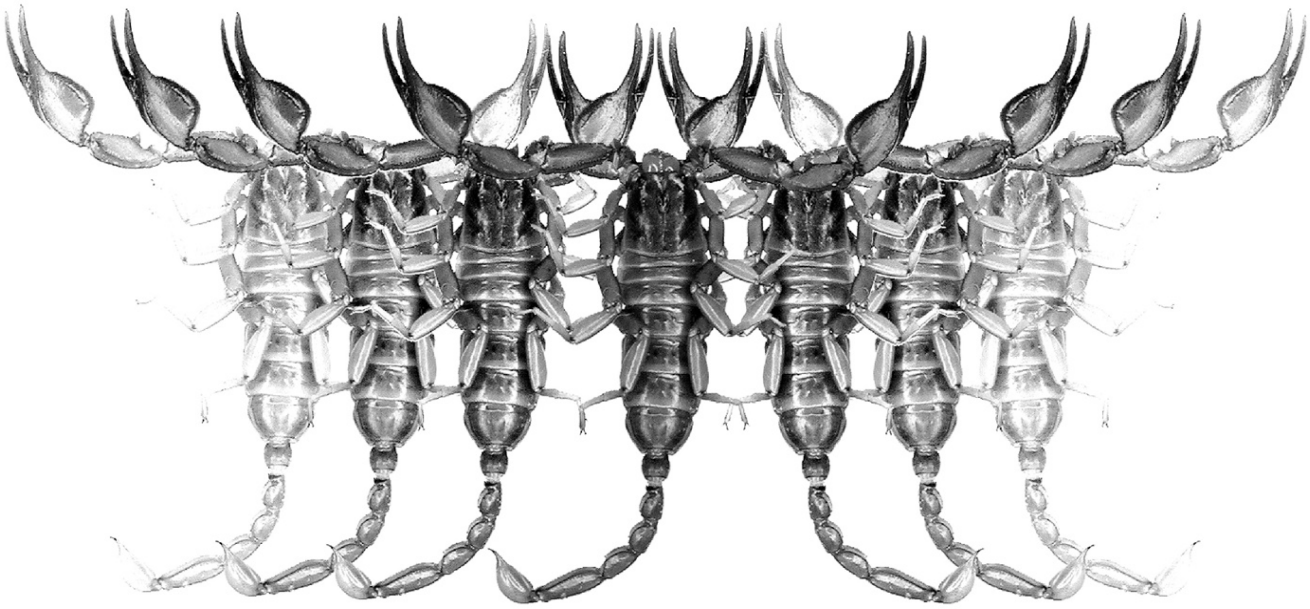

Three new species of genus *Scorpiops* Peters, 1861 from Tibet, China (Scorpiones: Scorpiopidae), with implications for the diagnostic values of qualitative characters

Victoria Tang, Kaichen Ouyang, Zhenbang Liu & František Šťáhlavský

August 2024 — No. 394

Euscorpius

Occasional Publications in Scorpiology

EDITOR: **Victor Fet**, Marshall University, **'fet@marshall.edu'**

ASSOCIATE EDITOR: **Michael E. Soleglad, 'msoleglad@gmail.com'**

TECHNICAL EDITOR: **František Kovařík, 'kovarik.scorpio@gmail.com'**

Euscorpius is the first research publication completely devoted to scorpions (Arachnida: Scorpiones). ***Euscorpius*** takes advantage of the rapidly evolving medium of quick online publication, at the same time maintaining high research standards for the burgeoning field of scorpion science (scorpiology). ***Euscorpius*** is an expedient and viable medium for the publication of serious papers in scorpiology, including (but not limited to): systematics, evolution, ecology, biogeography, and general biology of scorpions. Review papers, descriptions of new taxa, faunistic surveys, lists of museum collections, and book reviews are welcome.

Derivatio Nominis

The name ***Euscorpius*** Thorell, 1876 refers to the most common genus of scorpions in the Mediterranean region and southern Europe (family Euscorpiidae).

Euscorpius is located at: https://mds.marshall.edu/euscorpius/
Archive of issues 1-270 see also at: http://www.science.marshall.edu/fet/Euscorpius

(Marshall University, Huntington, West Virginia 25755-2510, USA)

ICZN COMPLIANCE OF ELECTRONIC PUBLICATIONS:

Electronic ("e-only") publications are fully compliant with ICZN (*International Code of Zoological Nomenclature*) (i.e. for the purposes of new names and new nomenclatural acts) when properly archived and registered. All ***Euscorpius*** issues starting from No. 156 (2013) are archived in two electronic archives:

- **Biotaxa,** http://biotaxa.org/Euscorpius (ICZN-approved and ZooBank-enabled)
- **Marshall Digital Scholar**, http://mds.marshall.edu/euscorpius/. (This website also archives all *Euscorpius* issues previously published on CD-ROMs.)

Between 2000 and 2013, ICZN ***did not accept online texts*** as "published work" (Article 9.8). At this time, *Euscorpius* was produced in two ***identical*** versions: online (*ISSN 1536-9307*) and CD-ROM (*ISSN 1536-9293*) (laser disk) in archive-quality, read-only format. Both versions had the identical date of publication, as well as identical page and figure numbers. ***Only copies distributed on a CD-ROM*** from ***Euscorpius*** in 2001-2012 represent published work in compliance with the ICZN, i.e. for the purposes of new names and new nomenclatural acts.

In September 2012, ICZN Article 8. What constitutes published work**,** has been amended and allowed for electronic publications, disallowing publication on optical discs. From January 2013, ***Euscorpius*** discontinued CD-ROM production; only online electronic version (ISSN 1536-9307) is published. For further details on the new ICZN amendment, see http://www.pensoft.net/journals/zookeys/article/3944/.

Publication date: 21 August 2024

http://zoobank.org/urn:lsid:zoobank.org:pub:72042F76-74B4-4F78-BDA6-988987C345DE

Euscorpius — Occasional Publications in Scorpiology. 2024, No. 394

Three new species of genus *Scorpiops* Peters, 1861 from Tibet, China (Scorpiones: Scorpiopidae), with implications for the diagnostic values of qualitative characters

Victoria Tang[1], Kaichen Ouyang[2], Zhenbang Liu[3] & František Šťáhlavský[4]

[1]Zhangyang Rd. 200120, Pudong New District, Shanghai, China; email: jibril.flueqel@gmail.com
[2]Huancheng West Rd., Xishan District, Kunming, Yunnan, China; email: 2936459671@qq.com
[3]Youjiang Medical University for Nationalities, Baise, Guangxi, China; email: maziyuu.helgen@gmail.com
[4]Department of Zoology, Charles University, Viničná 7, CZ-128 44 Praha 2, Czech Republic; email: frantisek.stahlavsky@natur.cuni.cz

http://zoobank.org/urn:lsid:zoobank.org:pub:72042F76-74B4-4F78-BDA6-988987C345DB

Summary

Three new species of genus *Scorpiops* Peters, 1861 are described from Tibet Autonomous Region, China. *S. deshpandei* **sp. n.** is described based on an adult male and an immature pair collected from Mêdog County, Nyingchi, with additional molecular evidence substantiating its validity against *S. longimanus* Pocock, 1893. *S. kovariki* **sp. n.** is featured by a single adult female from Zayü. This species is only weakly supported by its genetic distance from *S. jendeki* Kovařík, 1994, but empirical understanding of the morphological variation in *Scorpiops* species motivated us to consider them as distinct. *S. matthewi* **sp. n.** is based on three adult females, all collected from Xigazê. Its species delineation is based solely on morphological characteristics due to the lack of material of its morphological relative (*S. rufus* Lv & Di, 2023). New specimens of *S. margerisonae* Kovařík, 2000 are obtained from Nyêmo, Lhasa, and compared with *S. wrzecionkoi* Kovařík, 2020. A new term, "ocular islet", is introduced to portray the periocular morphology of *Scorpiops* median ocelli, categorized into four preliminary types. Finally, a comparative matrix summarizing the quantitative and qualitative diagnostic characters of Tibetan *Scorpiops* species based on preceding publications is provided.

Introduction

The Tibet Autonomous Region (or Xizang) of China is a vast territory that harbors a very rich scorpiofauna. To date, 31 species (excluding two records of dubious authenticity) belonging to 7 genera (*Hottentotta*, *Langxie*, *Reddyanus*, *Chaerilus*, *Scorpiops*, *Tibetiomachus* (*nomen dubium*), and *Deccanometrus*) across 5 families (Buthidae, Chaerilidae, Scorpiopidae, Hormuridae, and Scorpionidae) have been described/recorded from there (Tang, 2023; Lv & Di, 2023; Ythier, 2024). The genus *Scorpiops* Peters, 1861 includes the majority of those species (17/30 spp. of this genus in China), followed by *Chaerilus* Simon, 1877 (8/8 spp. of this genus in China). *S. tibetanus* Hirst, 1911 was the first species of this genus described from Tibet (Qüxü County, Lhasa). Since 2000, an increasing number of new species, alongside several new records (e.g., of *S. bhutanensis* Tikader & Bastawade, 1983; Lv & Di, 2022a) have been documented. As posited by Tang (2023: 48), the inclusion of two species, *S. hardwickii* (Gervais, 1843) and *S. petersii* Pocock, 1893, in the Tibetan records may be erroneous. In the last two years, two new species were described from Xigazê (or Rikaze, Shigatse) City, namely *S. lourencoi* Lv & Di, 2022 and *S. rufus* Lv & Di, 2023.

During a recent expedition to Tibet, the second author (a.k.a. Tongtong) collected several unidentified *Scorpiops* specimens from different localities within this region, sending nine of them to the first author. Subsequent scrutiny by the first author revealed that two specimens (from Nyêmo, Lhasa) were conspecific with *S. margerisonae* Kovařík, 2000, originally described from an unknown locality in Tibet based on an adult male. This discovery represents a new geographical occurrence for the species. However, the remaining seven specimens could not be unambiguously assigned to any known species. We tend to refrain from uncritically and hastily describing new species to avoid taxonomic inflation (Wüster et al., 2021), since the scarcity of specimens often leads to biased and/or erroneous new species description (Tang et al., 2024). Nevertheless, drawing on the investigator's experiential insights, in tandem with the known distribution and morphological characters of its congeners, such description can be supported insofar as unique qualitative and/or non-overlapping (or nearly so) quantitative characters are identified (as already seen in *Qianxie solegladi* Tang, 2022 and *Scorpiops tongtongi* Tang, 2022), preferably bolstered by additional molecular evidence. Following a comprehensive comparison with the descriptions and illustrations of known congeners, we propose these as three, distinct new species: *S.*

deshpandei **sp. n.**, *S. kovariki* **sp. n.** and *S. matthewi* **sp. n.** The validity of *S. deshpandei* **sp. n.** is further fortified by DNA analysis, leveraging available molecular data from the most closely related species exhibiting the highest morphological resemblance (*S. longimanus* Pocock, 1893). Regrettably, such molecular insights remain elusive for the putative relative of *S. matthewi* **sp. n.**, whereas in *S. kovariki* **sp. n.**, such between-species genetic divergence is low. Consequently, our differentiation solely (or mainly) relies on several unique morphological traits. The current study raises the number of *Scorpiops* species in China to that of 34, including a neglected species, *S. vonwicki* Birula, 1913. Conclusively, 21/35 (60%) scorpion species from Tibet are represented by the genus *Scorpiops*.

Methods, Material & Abbreviations

Morphology. Nomenclature and measurements follow Tang (2023), where problems associated with chela length and width measurements, and finger dentition differentiation have been elaborated. Standardized measurements of chela require leveling the condylar axis. Unstandardized measurement of chela depth is derived from two opposing surfaces: the plane defined by the dorsomedian and digital carinae, and the other defined by the ventromedian and interomedian carinae. Unless noted, all measurements are standardized; unstandardized values denoted with a prime at the right above corner (e.g., Ch-D', unstandardized chela depth). Total length is the summation of all somatic segments. Meristics for each specimen are expressed as "left count/right count". To clarify, the antecedent papers of the first author defined the left-right orientation in ventral view for pectinal tooth count (PTC), otherwise dorsally, both with the anterior end of the animal directed upwards. However, from an anatomical perspective, such left PTC represented the count for the intrinsic right pectine, and vice versa. The present paper hence redefined left and right pectines as well as their counts in alignment with all the other anatomical structures; this approach will be followed in the future papers. While both methodologies have been applied by other authors, it is not our current objective to rectify the prevalent confusions in scorpiology terminologies. Readers are free to switch the data as they see fit. Morphometrics in the diagnoses are based on all examined specimens unless specified. Only age-independent characters of immature specimens are incorporated into the diagnosis. Finger dentition color markings: inner accessory denticles = yellow, median denticles = green, inner denticles = blue, outer denticles = red. Qualitative terminology explanation: (1) "undulate", proximal lobe present on dentate margin of pedipalp movable finger; (2) "annular ring developed", circumference constricted at vesicle-aculeus juncture; (3) "anteromedian notch", the emargination at the anteromedian margin of carapace.

Materials. All specimens were collected by the second author, a Chinese enthusiast of nature and a trustworthy friend of the first author, who has been constantly providing Chinese scorpion materials for the first author. Two of the specimens (immature male *S. deshpandei* **sp. n.** and adult male *S. margerisonae*) were preserved in ethanol when received by the first author. Two paratypes of *S. matthewi* **sp. n.** were later sent to the first author during the finalization of this paper before which they were reared by the second author: one had died due to dehydration and one was on the edge of demise. The third paratype also died and was deposited in the personal collection of the second author, which was not directly examined by the first author. Holotypes of all new species were alive before they were euthanized for illustrative photography. Routine examination procedure follows Tang (2023). Leg tissues of all holotypes were preserved in 99% ethanol and sent to Charles University, Czech Republic. An additional specimen of *S. jendeki* Kovařík, 1994 collected by a local resident in Mengyang Town (Lianghe County, Dehong Prefecture, Yunnan Province) was included in the same material series for DNA sequencing. The third author was responsible for image matting, and the fourth author conducted molecular analyses. Supplementary photographs of type specimens and other specimens can be downloaded from the corresponding publication page of this paper on ResearchGate (a PDF file attached under the tab "Linked data"): www.researchgate.net/profile/Victoria-Tang-8/research, where unedited trichobothrial patterns are visible on the alternative pedipalp of the holotypes.

DNA sequencing and genetic distances calculation. This part was performed by the fourth author. Whole genomic DNA was extracted from leg muscle tissue using the E.Z.N.A. Tissue DNA Kit (Omega Bio-tek, Inc., Georgia) following the manufacturer's protocol. Partial fragments of two mitochondrial genes were amplified with the following primer combinations: Cytochrome oxidase I (*cox1*): C1-J-1490/C1-N-2198 (Folmer et al., 1994) and 16S rDNA (*16S*): 16Sbr/16SR (Simon et al., 1994; Gantenbein et al., 1999). The PCR conditions follow Štundlová et al. (2019). The PCR products were purified using a Gel/PCR DNA Fragments Extraction Kit (Geneaid, Taiwan) and sequenced by Macrogen Europe B.V. (The Netherlands). The obtained chromatograms were assembled, edited, and aligned in Geneious Prime 2022.1.1. All new DNA sequences were deposited in GenBank (www.ncbi.nlm.nih.gov/), with the following accession numbers [cox1/16S]: *Scorpiops jendeki* (specimen code: S2718, China, Yunnan. Lianghe, Dehong Prefecture), PQ149985/PQ149976; *S. tongtongi* (specimen code: S2684, China, Yingjiang County, near Rongshuwang), PQ149983/PQ149974; *S. yangi* (specimen code: S2717, China, Yunnan. Malipo County, Wenshan Prefecture), PQ149984/PQ149975; *S. deshpandei* **sp. n.** (specimen code: S2720), PQ149986/PQ149977; *S. kovariki* **sp. n.** (specimen code: S2721), PQ149987/PQ149978; *S. matthewi* **sp. n.** (specimen code: S2722), PQ149988/PQ149979. For the comparison of the analyzed samples, we also included already published sequences from *S. anthracinus* [MW269416/MW250317; MW269420/MW250320; MW269421/MW250321], *S. leptochirus* [MW269410/MW250310], *S. montanus* [MW269419/MW250319] (Šťáhlavský et al.,

2021), and *S. longimanus* [n.a./MW665151; n.a./MW665152; n.a./MW665153; n.a./MZ057759; n.a./MZ057760; n.a./MZ057758] (Malsawmdawngliana et al., 2022). The final alignments lengths were set to 597 bp for *coxI* and 311 bp for *16S*. Their uncorrected pairwise distances were calculated in MEGA version 11 (Tamura, Stecher, and Kumar 2021) (Table 3).

Abbreviations. TL, total length (in mm); Ch-L/W, length to width ratio of pedipalp chela; Ch-L/D, length to depth ratio of pedipalp chela; ChL/CaL, chela length to carapace length ratio; ChW/CaL, chela width to carapace length ratio; T-L/D, length to depth ratio of telson; PTC, pectinal tooth count; PVTC, pedipalp patella ventral trichobothrium count; PETC, pedipalp patella external trichobothrium count; IAD, inner accessory denticle; MD, median denticle; ID, inner denticle; OD, outer denticle; Eb_3 pos., relative position of trichobothrium Eb_3 on pedipalp chela manus (definition follows Kovařík et al., 2020: 8); P, pectine morphology (definition follows Kovařík et al., 2020: 21).

Specimen Depositories. FKCP, personal collection of František Kovařík, Prague, Czech Republic (will in future be merged with the collections of the National Museum of Natural History, Prague, Czech Republic); VT, personal collection of Victoria Tang, Shanghai, China.

Periocular morphology of median ocelli

A new term, "ocular islet" (eye island, the "isle" upon which the median ocelli situate), associated with the median ocelli, is introduced and defined as the entire convex structure confined within and delimitated by the circumocular sulcus, typically streamlined in profile. It was previously referred to as the "ocular tubercle" (or "ocular tubercle coverage") in Tang (2022b, 2022c, 2023), a term now strictly denoting the immediate periocular structure of median ocelli (primarily constituted by the superciliary carinae), approximately located at the center of the ocular islet. Considering that the term "tubercle" by definition refers to a oval nodule, this decision was made *a fortiori* based on semantic propriety. The introduction of the term "ocular islet" aims to characterize interspecific disparities potentially diagnostic at the species level, as observed during the current investigation of our new species.

The median ocular tubercle can be parameterized by its relative location within the ocular islet, length to width ratio (shape), prominence and smoothness of superciliary carinae, distinctiveness (or depth, width) of interocular sulcus, and relative size of ocular socket (essentially that of the median ocelli). Subtracting the ocular tubercle from ocular islet renders two opposing, subtriangular areas, denoted as "anterocular subislet" and "postocular subislet". These two subislets vary interspecifically in shape (relative length or area), and density and coarseness of granules. However, if one were to juxtapose the periocular structure of Scorpiopidae with those of the other taxa, it becomes apparent that these subislets are *de facto* fused superciliary carinae in a homologous sense, where a prominent interocular sulcus traverses the entire carapace surface. In such cases, identifiable subislets, occasionally even the median ocular tubercle itself, are non-existent. Ergo, our terminology is restrained exclusively to the distinct morphology observed in Scorpiopidae. En bloc, the morphology of the ocular islet can be scored by the abovementioned variables and classified into different types, potentially serving as diagnostic criteria for *Scorpiops* species (cf. Tang, 2023: figs. 137–154).

In order to enhance the comprehensiveness and applicability of our definitions for the ocular islet types, ensuring minimal ambiguity in their identification (i.e., no character gradient between types), a survey of 91 out of 110 currently valid *Scorpiops* species (including the three new species described herein) was conducted. The investigated species were categorized under different types and included in another PDF file under the same tab alongside the supplementary file (see Methods). However, this examination primarily reliant upon published photographs, which suffered from several nuisances. The bias during the tentative allocation of those species to different types stemmed from the unfavorable resolution or light condition (sufficiency and/or direction). Additionally, UV fluorescence imaging may result in misleading visual effects due to variability in fluorescence intensity across different cuticle areas. Consequently, our resultant classification is only provisional which may also not cover the gamut of all possible variants, necessitating amendments based on the inspection of authentic specimens.

For the purposes of descriptive taxonomy at species level, we register the following empirical definitions of preliminary ocular islet types (adjective descriptors only in relative sense):

OI-1 (Type 1). Ocular tubercle distinct within ocular islet, rounded or elliptical in profile; subislets weakly (sparsely) or finely granular, planar; interocular sulcus absent or weak to moderate (when present); superciliary carinae smooth or nearly so, may also be punctate; ocular sockets typically small. **Representative taxa**: *S. atomatus* (Qi et al., 2005), *S. demisi* Kovařík, 2005, *S. ingens* Yin et al., 2015, *S. lindbergi* Vachon, 1980, *S. lourencoi*, *S. luridus* Qi et al., 2005, *S. pachmarhicus* Bastawade, 1992, *S. rufus*, *S. songi* Di & Qiao, 2020, *S. spitiensis* Zambre et al., 2014, *S. tibetanus*, *S. tongtongi*, *S. vonwicki*, *S. wrzecionkoi* Kovařík, 2020, and *S. zhui* Lv et al, 2023.

OI-2 (Type 2). Ocular tubercle distinct within ocular islet, rounded in profile; subislets weakly (sparsely) or finely granular, elongated and somewhat elevated; interocular sulcus absent or weak (when present); superciliary carinae smooth or nearly so; ocular sockets typically small. **Representative taxa**: *S. deccanensis* Tikader & Bastawade, 1977, *S. lioneli* Sulakhe et al., 2021, *S. maharashtraensis* (Mirza et al., 2013), *S. nagphani* Sulakhe et al., 2021, *S. neera* Sulakhe et al., 2021, *S. tenuicauda* Pocock, 1894, and *S. vrushchik* Sulakhe et al., 2021.

OI-3 (Type 3). Ocular tubercle less distinct within ocular islet, moderately elevated and merged with granular ridges of antero- and postocular subislets; subislets moderate to elongated, coarsely granular; interocular sulcus distinct;

superciliary carinae smooth, engraved or granular; ocular sockets typically moderate to large. **Representative taxa**: *S. bastawadei* Kovařík et al., 2020, *S. birulai* Kovařík et al., 2020, *S. dii* Kovařík et al., 2020, *S. kautti* Kovařík et al., 2020, *S. krabiensis* Kovařík et al., 2020, *S. novaki* (Kovařík, 2005), *S. prasiti* Kovařík et al., 2020, *S. sherwoodae* Kovařík et al., 2020, and *S. viktoriae* (Lourenço & Košulič, 2018).

OI-4 (Type 4). Ocular tubercle indistinct within ocular islet, flattened and fused with antero- and postocular subislets; subislets short, smooth to finely granular; interocular sulcus moderate to weak; superciliary carinae absent or smooth to engraved (when present); ocular sockets large. **Representative taxa**: *S. dunlopi* Kovařík et al., 2020, *S. neradi* (Kovařík et al., 2013), *S. pakseensis* Kovařík et al., 2020, *S. phatoensis* Kovařík et al., 202,0 and *S. solegladi* Kovařík et al., 2020.

Suggestive abbreviations: MOT, median ocular tubercle(s); OI, ocular islet(s); AOSI, anterocular subislet; POSI, postocular subislet; SCC, superciliary carina(e); IOS, interocular sulcus; COS, circumocular sulcus. A scheme is provided to illustrate our definitions for those terms (Fig. 128). Adopted henceforth.

The MOT typically resides centrally within the OI, occasionally exhibiting an anterior position, a feature consistent across all types. The shape or conspicuousness of the MOT is primarily decided by the elevation of the two subislets. The length of the MOT is defined along the rostrocaudal axis, while its width is defined parallel to the mediolateral axis. In Type 1 ocular islets, the MOT would seem fairly distinguished as the two subislets are planar and weakly granular while the tubercle itself is highly elevated. Depending on the slope from the SCC towards the subislets, its peripheral profile may display a rounded or elliptical shape. For instance, in species like *S. wrzecionkoi* (Figs. 133–134), a steeper descent results in a rounded profile, while a moderate slope yields an elliptical profile, as seen in *S. kovariki* **sp**. **n**. and *S. matthewi* **sp**. **n**. (Figs. 131–132).This within-type character gradient suggests the potential existence of subtypes. Conversely, if the two subislets are strongly granular and elevated, as typically manifested by Type 3, the profile of MOT would then appear less distinct. In this case, the SCC may merge with an anterior ridge and a posterior ridge formed by subislet granules extending to the opposing extremities of the OI (e.g., *S. deshpandei* **sp**. **n**. and *S. novaki*; Figs. 130, 139). Similarly, in the Type 4 ocular islet, where the MOT is not strongly elevated, its distinctiveness diminishes. However, the apparent fusion between MOT and elevated subislets was also seen in taxa that define Type 2. This type of OI appear to be intermediate between Type 1 and Type 3. It shares the elevated subislets as observed in the latter, while a closer resemblance with the former is represented by an absent to weak IOS, smooth SCC and small ocular sockets. While there is some degree of fusion between the MOT and elevated subislets, the MOT remains conspicuous and rounded in profile due to the subislets being narrower and more granular. When viewed distantly, the Type 1 ocular islet is dominated by the short, rounded or elliptical MOT (cf. Figs. 131–138), while those corresponding to Type 3 may appear rhomboid due to the elevated, granulated subislets that enhance the overall visual effect (cf. Tang, 2023: figs. 138–145, 146–154). On that account, ambiguity may occur when attempting to discriminate the MOT from the OI in Type 3 ocular islets. Suggestively, an ellipsoid can be fitted to envelope the MOT with its profile partially determined by the lateral contour of the median ocelli from the dorsal view.

The surface texture of SCC can vary from smooth, granular, engraved to punctate. Granular or engraved carinae are usually seen in taxa with strongly granulated subislets (Type 3), while punctate carinae are limited to taxa with rounded ocular tubercles within Type 1. On the contrary, smooth carinae are found across all types. The notability of IOS *per se* hinges on the degree of fusion between SCC (or their development). Highly fused SCC are often observed in MOT with a rounded profile, while a lesser degree is noticed in those with an elliptical profile (both classified under Type 1). On the other hand, the evident separation is often discovered in taxa with strongly granular subislets (Type 3), or planar MOT (Type 4, which are surrounded by weakly to finely granulated subislets). It is noteworthy that a greater relative distance between the median ocelli does not necessarily entail the presence of a deep IOS, although that may often be the case. *S. furai* Kovařík, 2020, *S. grosseri* Kovařík, 2020, *S. harmsi* Kovařík, 2020, *S. kejvali* Kovařík, 2020, and *S. tryznai* Kovařík, 2020, tentatively classified under Type 1, appear to be featured with a different combination of morphology as opposed to the ordinary Type 1 taxa: while their subislets appear to be planar and weakly granular, an ostensibly distinct IOS is visible, yet nonetheless confined within the sphere of MOT. This apparent within-type variation in the depth of IOS indicates the plausible existence of subtypes, or even separate types. We view the amalgamation of the multiplicity of Type 1 ocular islet as a temporary expedient, instead of precipitately defining additional types that exhibit only limited nuances, which may, in hindsight, prove unnecessary. Relatively large ocular sockets (or median ocelli) appear to be more common in taxa with a less distinctive MOT (Type 3 and Type 4).

Besides the density and coarseness of granules discussed in association with other structures as above, the subislets are particularly featured by their shape. The COS is smooth (or finely granular), often showing stronger UV excited fluorescence, which facilitates the discrimination of the subislet profile. The subislets are somewhat triangular, meaning that their bilateral outlines would converge towards the rostrocaudal axis to the extremity. We propose that its shape can be quantitatively delineated by several parameters: (1) the relative length of each subislet with respect to the length of MOT; (2) the average width (mean) of each subislet; (3) the maximum width (upper limit) of each subislet; (4) the width at the middle section (median) of each subislet. There may be considerable intraspecific variations that could swamp the between-species difference. Therefore, those parameters are only aimed for a quantified definition for the OI type where different species can be simply classified under the same type.

Figures 1–2. *Scorpiops deshpandei* **sp**. **n**., holotype male, habitus in dorsal (1) and ventral (2) views, under white light. Scale bar = 10 mm.

The four types may be associated with the ratiometrics of pedipalp chela and other morphological aspects. Type 4 ocular islet appears to demonstrate the strongest correlation with this aspect: it is only found in small sized taxa, typically with cubic chelae and short fingers (except for *S. solegladi*), mostly from Thailand. Likewise, Type 3 ocular islets are consistently observed in species with coarsely granular cuticle and moderately to highly elongated chelae (except for *S. yagmuri* Kovařík, 2020). However, Type 1 ocular islets present complexities where species categorized under OI-1 possess either short and stout, or long and flattened chelae. Notably, the short and stout chelae were only seen in OI-1, whereas the long and flattened chelae were ubiquitous in OI-2, observed in species from India and Pakistan.

Due to the apparent presence of within-type character gradient, those preliminary types may be subject to finer classifications contingently. We add a caveat here that the periocular morphology may be subject to a certain extent of intraspecific variation, thus any perceived minor difference should not be exaggerated for species discrimination unless they are proved stable. The new terminology and type definition proposed here only serve to group several (currently, four) main categories of *Scorpiops* species delimited by the periocular morphology. Our current objective is to proffer a normative framework for the description of those structures in our new species. Further morphogeometric analyses based on a thorough examination of specimens are required to objectively confirm their categorization and diagnostic merit for the genus *Scorpiops*. Moreover, the relative size/coverage of OI or MOT on the carapace may offer additional informative insights. Those potential utilities have been implied in the previous study on Yunnan *Scorpiops* (Tang, 2023).

Genetic distances

To support the species delimitation of the *Scorpiops* species, we calculated uncorrected pairwise genetic distances for two mitochondrial genes, *coxI* and *16S* (Table 3). Both genes displayed high interspecific distances among the analyzed taxa, typically ranging from 9.2% to 14.9% for *coxI* and from 7.4% to 13.5% for 16S. The slightly lower p-distances of *16S* compared to *coxI* are evident especially in the values between *Scorpiops kovariki* **sp**. **n**. and *S. jendeki* (1.9% for 16S and 7.7% for cox1). For *16S*, such low p-distances actually correspond to intraspecific variability observed within *S. longimanus* (p-distances: 0.0%–4.8%, mean 3.2%) (Table 3). Slightly lower p-distances were also detected between *S. longimanus* and *S. deshpandei* **sp**. **n**. (p-distances of *16S*: 5.1%–7.7%, mean 6.5%).

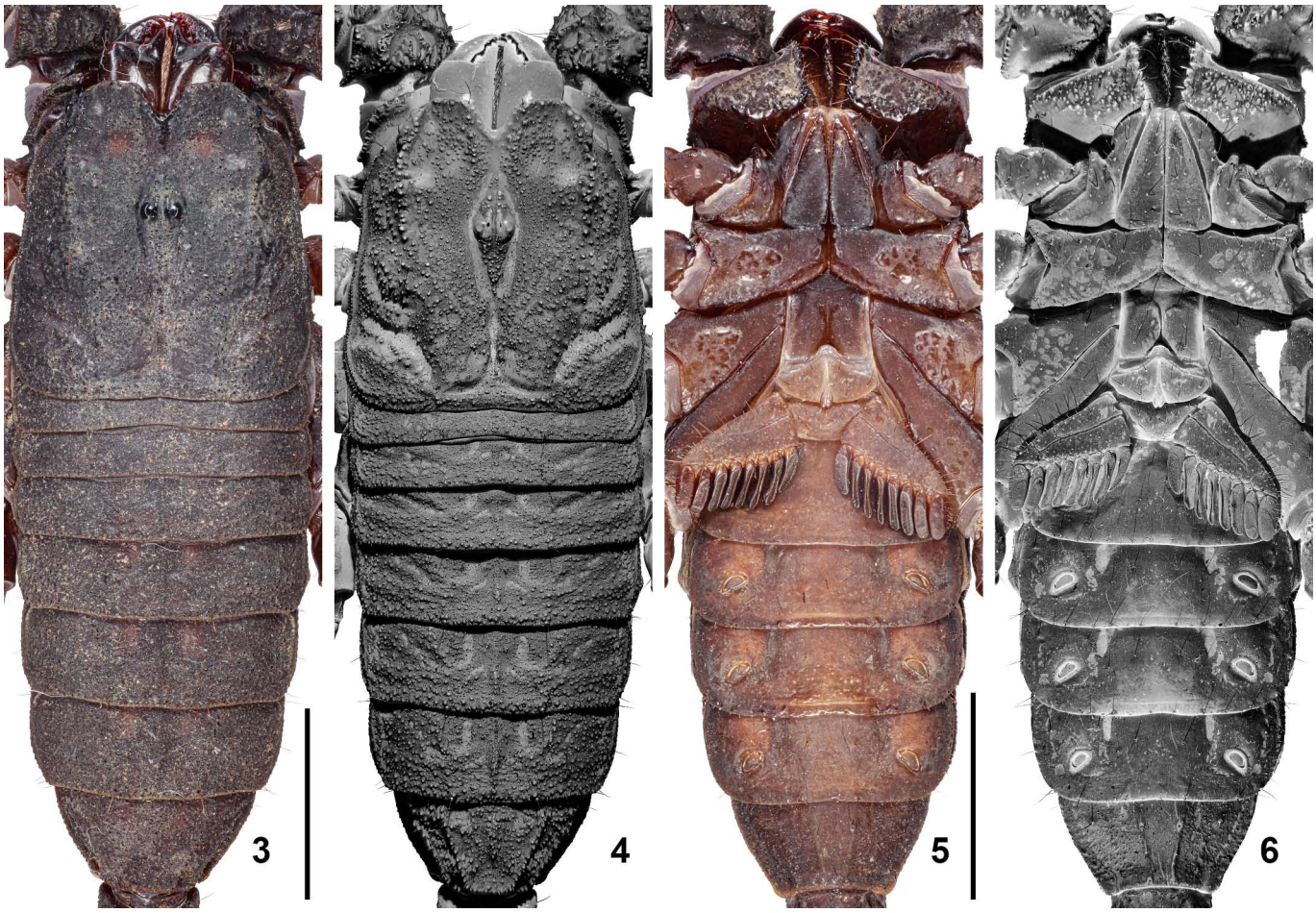

Figures 3–6: *Scorpiops deshpandei* **sp. n.**, holotype male, prosoma and mesosoma. **Figures 3–4**. In dorsal view, under white (3) and UV (4) light. **Figures 5–6**. In ventral view, under white (5) and UV (6) light. Scale bar = 5 mm (Figs. 3, 5).

Systematics

Family Scorpiopidae Kraepelin, 1905
Scorpiops Peters, 1861

***Scorpiops deshpandei* sp. n.**
(Figures 1–38; Tables 1–2)
http://zoobank.org/urn:lsid:zoobank.org:act:1562EED8-C72E-407F-A311-5D70C2DDE2AF

Type locality and type depository. **CHINA**, ***Tibet Autonomous Region***, Nyingchi (or Linzhi, Nyingtri) prefecture-level City, Mêdog (or Motuo, Pemako) County, Drepung (or Beibeng, Baibung) Township (or Beibengxiang), 29°13'49.0"N 95°10'45.8"E (29.23027117°N 95.17938118°E), 1523 m a. s. l.; VT.

Type material. **CHINA**, ***Tibet Autonomous Region***, Nyingchi prefecture-level City, Mêdog County, Drepung Township, 29°13'49.0"N 95°10'45.8"E, 1523 m a. s. l., 19 July 2023, 1♂ (holotype), 2 juvs. ♂♀ (paratypes), leg. Tongtong.

Etymology. The specific epithet is a patronym in honor of Indian scorpiologist Shubhankar Deshpande, a friend of the first author and a passionate, responsible scorpion enthusiast focusing on the taxonomy of *Scorpiops* and *Isometrus* Ehrenberg, 1828. The nexus between the concrete species and and its nomenclature was established based on its evident resemblance to the Indian congener, *S. longimanus*. Chinese equivalent: 德氏类蝎 (roughly as "Deshpande's resemblant scorpion" in English; see Tang (2022a) for the rules of designation).

Diagnosis. Total length ca. 54 mm for male. Base color uniformly reddish brown to brownish black; chela manus, telson and parts of legs slightly brighter, genital plate, pectinal lamellae and venter brownish, pectinal teeth dark brown (in vivo, for holotype). Cuticular surface matte and moderately granular. Carapace with anteromedian notch triangular; ocular tubercle not distinct within ocular islet; ocular subislets moderate in length and coarsely granular; interocular sulcus distinct; superciliary carinae granular. Cheliceral fixed finger with basal and median denticles forming into a bicuspid trunk. PTC 8 in male and 7 in female; pectines with 3 marginal and 1 middle lamellae (P4); fulcra present; sternites III–VI matte, VII granular with four distinct carinae. Pedipalp patella with strong prolateral apophysis; 17–18 external and 7–8 ventral trichobothria. Chela with 4 *V* series trichobothria; Eb_3 located in middle of manus at nearly the same level as *Dt* (type B);

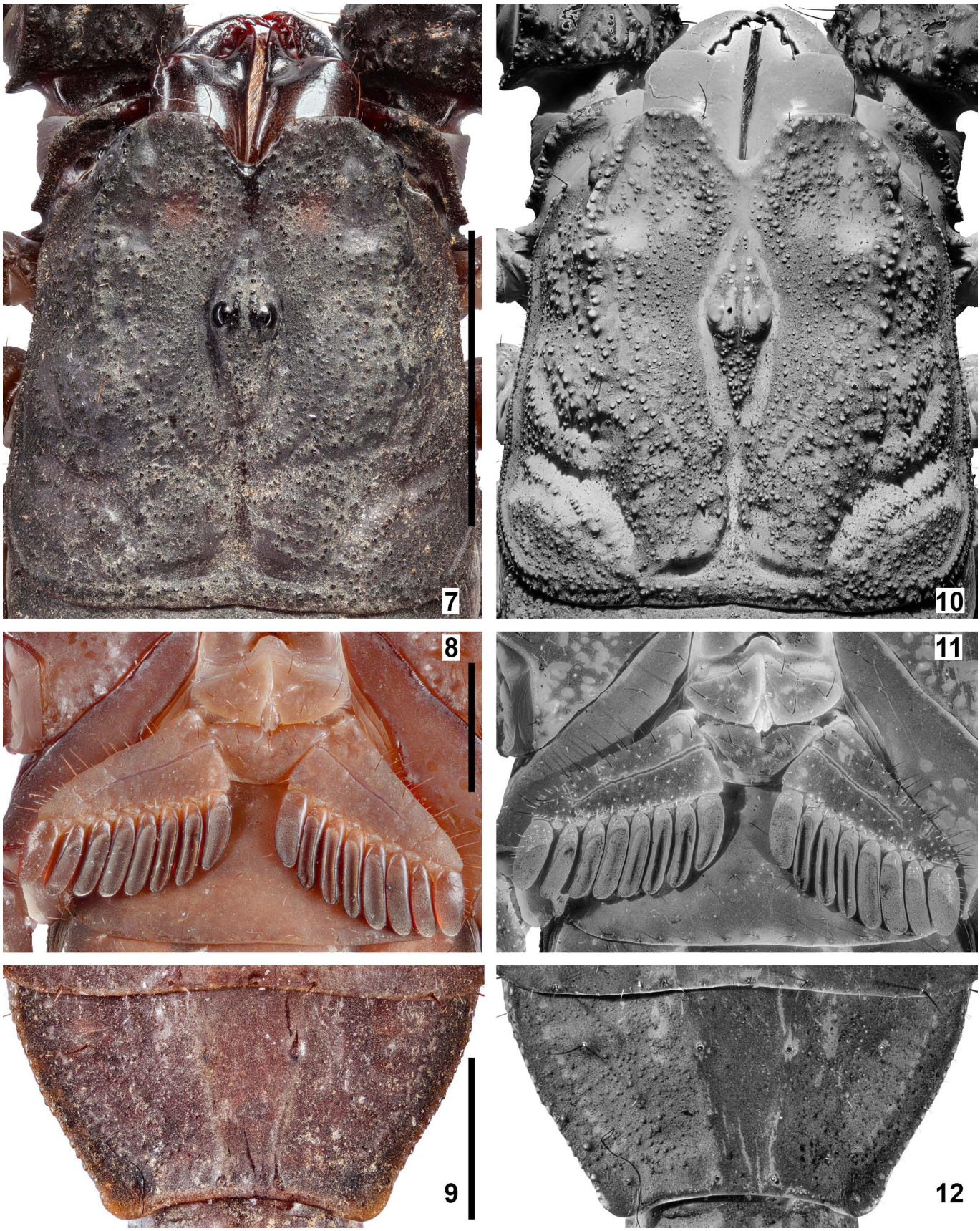

Figures 7–12: *Scorpiops deshpandei* **sp. n.**, holotype male, carapace (7, 10), pectines (8, 11) and sternite VII (9, 12). **Figures 7–9**. Under white light. **Figures 10–12**. Under UV light. Scale bar = 5 mm (Fig. 7), 2 mm (Figs. 8–9).

Dimensions (mm)		*Scorpiops deshpandei* **sp. n.** HT ♂	*Scorpiops kovariki* **sp. n.** HT ♀	*Scorpiops matthewi* **sp. n.** HT ♀
Carapace	L / W	8.43 / 8.21	4.84 / 5.11	7.94 / 7.98
Mesosoma	L	18.15	11.06	19.31
Tergite VII	L / W	3.8 / 5.85	2.15 / 4.37	4.21 / 6.57
Metasoma + telson	L	27.66	17.05	32.06
Segment I	L / W / D	2.79 / 2.76 / 2.11	1.58 / 2.12 / 1.57	3.55 / 3.1 / 2.56
Segment II	L / W / D	3.23 / 2.46 / 2.05	2.04 / 1.9 / 1.52	3.76 / 2.85 / 2.52
Segment III	L / W / D	3.52 / 2.22 / 1.96	2.22 / 1.78 / 1.49	4.12 / 2.83 / 2.58
Segment IV	L / W / D	3.84 / 1.99 / 2.11	2.59 / 1.56 / 1.41	4.75 / 2.67 / 2.54
Segment V	L / W / D	6.64 / 1.94 / 1.84	4.14 / 1.35 / 1.37	7.7 / 2.47 / 2.44
Telson	L / W / D	7.64 / 2.08 / 2.14	4.48 / 1.45 / 1.47	8.18 / 3.23 / 3.22
Pedipalp	L	39.24	15.73	27.6
Femur	L / W	10.95 / 3.65	3.8 / 1.68	6.7 / 3.05
Patella	L / W	9.17 / 4.16	3.84 / 1.85	6.66 / 3.21
Chela	L	19.12	8.09	14.24
Manus	L / W / D	11.7 / 4 / 3.97	4.93 / 3.36 / 2.93	8.64 / 5.13 / 4.69
Fixed Finger	L	7.42	3.16	5.63
Movable finger	L	9.52	4.36	8.09
Total	**L**	**54.24**	**32.95**	**59.31**
PTC	Left / Right	8 / 8	4 / 4	4 / 4

Table 1. Measurements of *S. deshpandei* **sp**. **n**., *S. kovariki* **sp**. **n**. and *S. matthewi* **sp**. **n**. Abbreviations: holotype (HT), length (L), width (W, in carapace it corresponds to posterior width), depth (D). Pedipalp length excludes trochanter length.

Ch-L/W ca. 4.78 in male. Dentate margin of movable fingers weakly undulate in male, with 13–14 OD, 83–97 MD, 51–65 IAD and 5–7 ID. Telotarsi of leg I–VI with 8–9 stout median ventral spinules nearly in a single row. Metasoma I–V with 10-8-8-8-7 carinae. Telson slender and relatively smooth; T-L/D ca. 3.57 in male; annular ring developed.

Description (♂).Overall habitus (Figs. 1–2), prosoma, mesosoma, metasoma and telson, chelicera, legs and hemispermatophore were photographed under white light. Additional UV fluorescence imaging was applied for prosoma and mesosoma. Pedipalp was photographed only under UV light given its lack of distinct color patterns.

Prosoma and mesosoma (Figs. 3–12, 24–25). *Prosoma*: Carapace with 3 pairs of lateral ocelli (two larger, one smaller); median ocular tubercle not distinct within islet, merged with granular ridges of antero- and postocular subislets; subislets moderated in length and coarsely granular, somewhat elevated; interocular sulcus distinct; superciliary carinae granular and gradually fused with subislets. Dorsomedian part of the carapace (ca. 2/3 of total area) planar, with anterolateral boundaries demarcated by coarse granules; lateral surfaces slanting downwards. Entire carapace densely covered with moderate granules, and adorned with lattice microstructures at non-granular regions; larger granules concentrated anteriorly at edges flanking anteromedian sulcus, and above and posterior to lateral ocelli; distinct carinae absent. Anterior margin of carapace with a prominent, triangular median notch leading to a shallow, smooth anteromedian sulcus; circumocular and posteromedian sulci smooth; lateral surfaces with a pair of moderate central lateral sulci and prominent posterior lateral sulci, both non-granular; posterior marginal sulcus deep. Chelicerae with dorsal surface smooth and ventral surface densely setose on 2/3 area; all denticles of cheliceral fingers sharp; basal and median denticles on fixed finger strongly conjoined on a common trunk. *Mesosoma*: Tergites I–III highly granular, VII coarsely granulated and pentacarinate; all tergites sparsely covered with small to moderate, pointed granules, becoming denser closer to posterior margins, with weak median carina indicated (more prominent on VI–IV while concealed by random granules on VII). Sternites III–IV smooth, with multiple macrosetae arrayed along the posterior margin, as well as two axisymmetric, curved furrows; sternite VII moderately granulated with two costate carinae; respiratory spiracles suboval. Genital operculum divided into two halves, with genital papillae at the base. Pectines with 3 marginal and 1 middle lamellae present; pectine teeth number 8/8; area of peg sensilla covers the majority of each pectinal tooth; fulcra present and developed; numerous fluorescent microsetae present.

Metasoma and telson (Figs. 26–29). Metasoma sparsely hirsute and granulated; carinae formed by moderately fused granules (costate-granular). Metasoma I with 10 carinae, II–IV with 8 carinae, and V with 7 carinae; median lateral carinae of metasoma II–III very weakly indicated at the distal part by granules, absent on IV; all carinae weakly serrated,

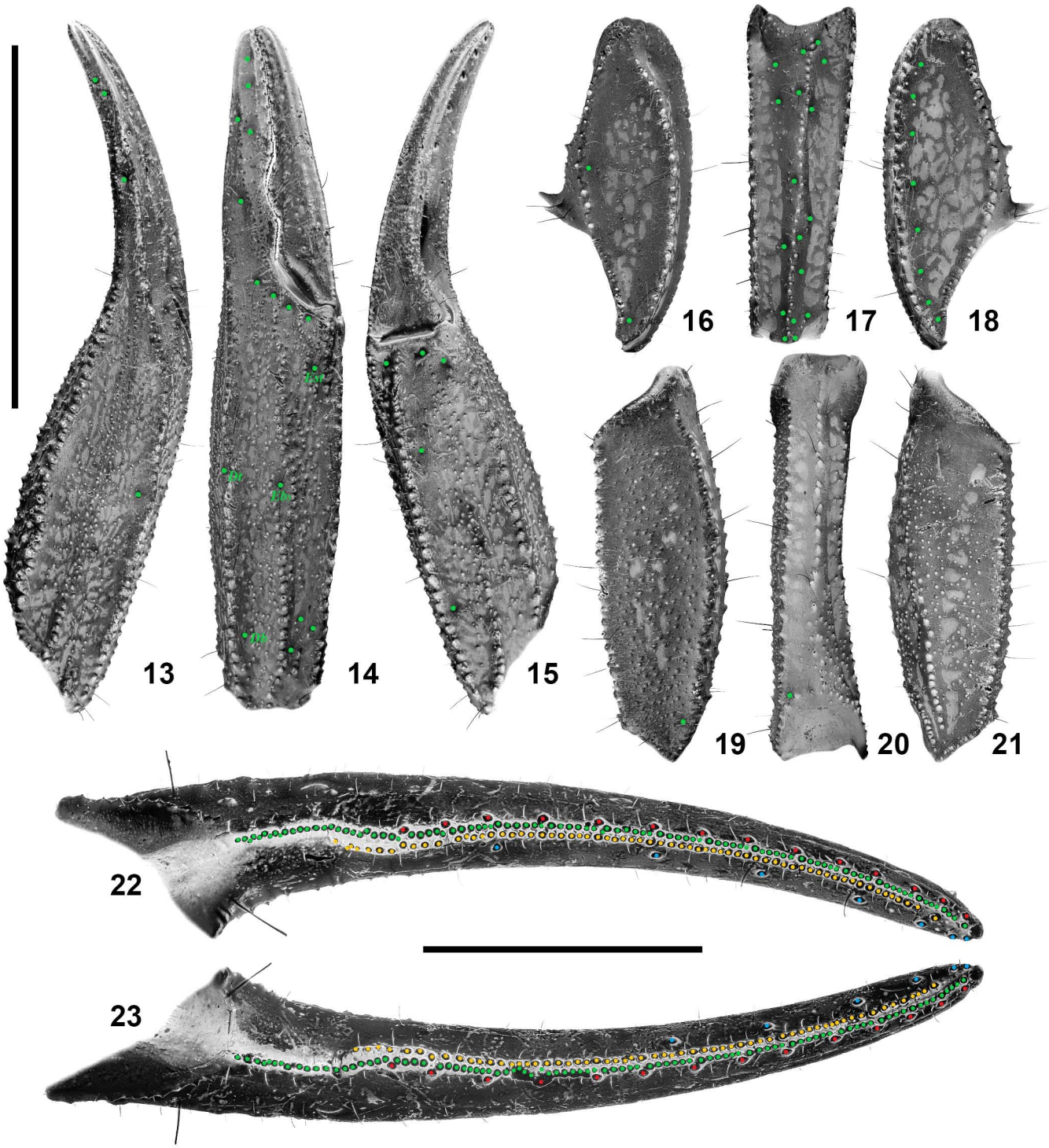

Figures 13–23. *Scorpiops deshpandei* **sp**. **n**., holotype male, pedipalp chela in dorsal (13), external (14) and ventral (15) views, patella in dorsal (16), external (17) and ventral (18) views, femur in dorsal (19), external (20) and ventral (21) views, left (22) and right (23) movable fingers in dorsal view, under UV light. Scale bar = 10 mm (Figs. 13–21), 3 mm (Figs. 22–23).

but stronger in ventromedian carina on metasoma V. Anal arch armed with sharp granules. Telson smooth, very sparsely hirsute, elongated and dorsally weakly concave; all surfaces nearly smooth, otherwise adorned by very fine granules; prominent annular ring developed. Vesicle with lateral surface furnished by one longitudinal sulci close to dorsal surface, and ventral surface with two parallel longitudinal sulci; all four sulci relatively shallow and basically smooth (covered with extremely minute granules). Aculeus smooth, short, very weakly curved (tip slightly broken).

Pedipalps (Figs. 13–23). Pedipalps very sparsely hirsute, intercarinal surfaces scattered with small to moderate granules and patches of lattice microstructures. Patella with 17/18(?) external (4 *et*, 4 *est*, 2/3(?) *em*, 2 *esb*, 5 *eb*) and 7/8

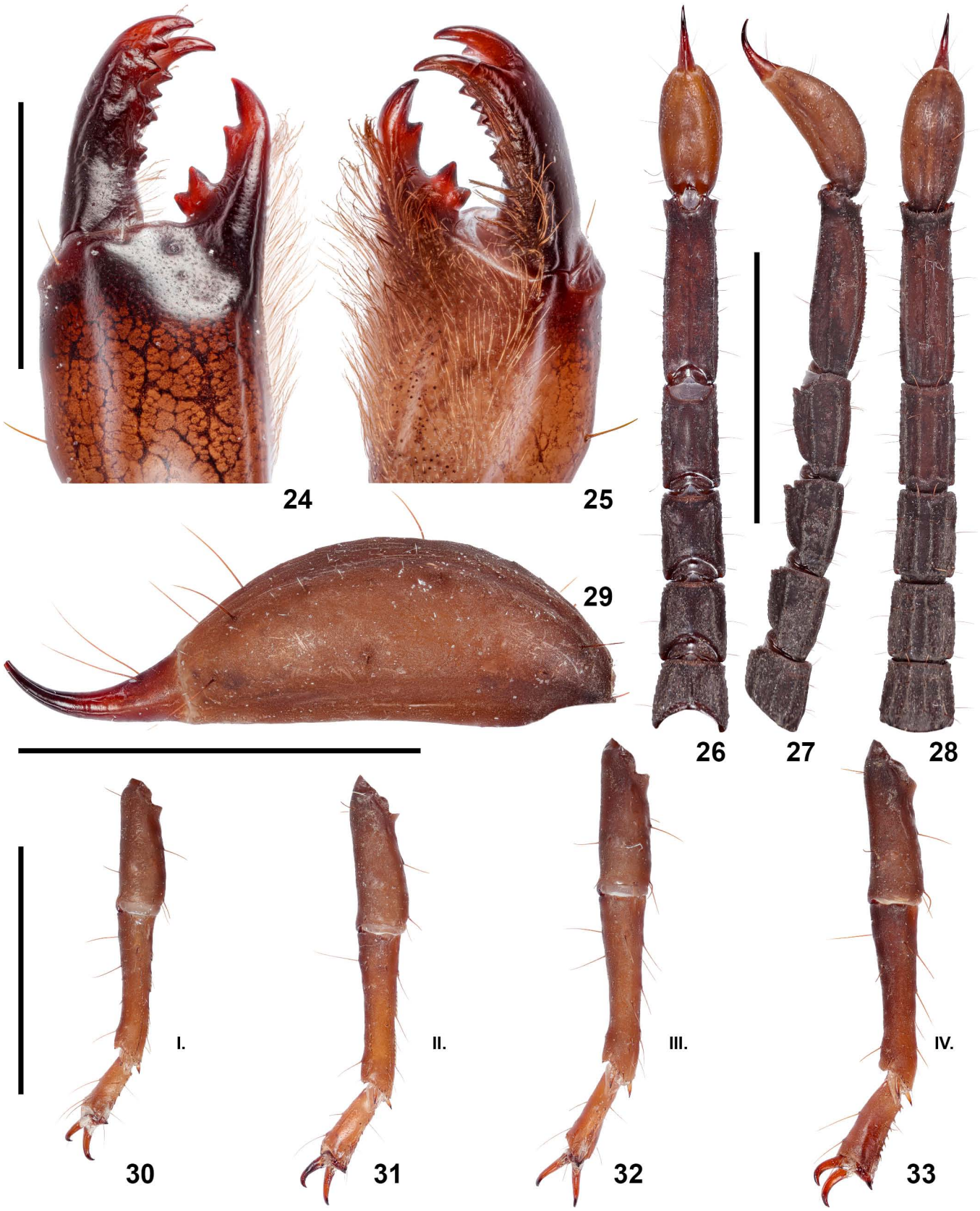

Figures 24–33. *Scorpiops deshpandei* **sp**. **n**., holotype male, left chelicera in dorsal (24) and ventral (25) views, metasoma and telson in dorsal (26), lateral (27) and ventral (28) views, telson in lateral view (29), left legs I–IV in retrolateral view (30–33), under white light. Scale bar = 2 mm (Figs. 24–25), 10 mm (Figs. 26–28), 5 mm (Figs. 29 horizontal, 30–33 vertical).

ventral trichobothria. Chela with 4 *V* series trichobothria; trichobothrium Eb_3 located in middle of manus at nearly the same level as *Dt* (Eb_3 more proximal). Femur with 5 highly granular carinae and a densely granulated dorsal surface; promedian carina obsolete, delineated by two larger granules; retroventral carina partially incomplete, respectively diffusing into random granules of the same size as adjacent intercarinal granules proximally and distally; other 4 carinae complete, formed by large, discrete granules. Patella with 5 granular carinae with finely and sparsely intercarinal surfaces; granules smaller on retromedian carina; granules form a weakly reticulate configuration on dorsal surface; prolateral surface with a triangular apophysis armed with two long spiniform granules. Manus moderately adorned with small intercarinal granules on all surfaces; all carinae granular; subdigital and ventroexternal carinae obsolete; dorsal secondary, external secondary and ventrointernal carinae relatively short, gradually diffusing to dispersed granules distally; granules on dorsal marginal, ventromedian and interomedian carinae larger. Dentate margin of movable fingers weakly undulate (proximal lobe present), adorned by 14/14 OD, 97/91 MD, 65/60 IAD (same size as MD) and 7/6 ID; IAD series creates a second row along MD series without obvious subdivisions.

Legs (Figs. 30–33). Tibia and tarsomeres of legs with several macrosetae not arranged into bristle combs. Basitarsi of legs I–II with two rows of dense, short spinules, but both absent on legs III–IV; a pair of pedal spurs present on the distal margin of all basitarsi. Telotarsi of legs I–IV with a row of short, stout ventromedian spinules (8–9 in number) of which two are always paired on the distal end. Ungues moderate in length, stout and curved. Carinae on femur and patella either finely granular or costate.

Hemispermatophore (Figs. 35–38). Lamelliform in profile. Distal lamina long, moderately slender; basally constricted, terminally coiled and tapered. Capsule conforms to 2-folds bauplan; distal posterior lobe marginally sclerotized and armed with ca. 12 denticles of which 4 located along the lateral edge; lateral hook entirely sclerotized, irregular in shape, apically sharpened; terminal membrane of sperm duct translucent but not spiculate; basal carina accords with Group 4 (Kovařík et al., 2020: 27), sclerotized and distally expended into a plate with polydentate basal crest bearing crown-like structure. Trunk broad with mid-axial rib dividing it into anterior and posterior halves, distal end of the axial rib connected to the sclerotized distal carina of the capsule by a narrow junction, truncal flexure absent. Pedicel (= foot, in Kovařík et al., 2020) broad, soft and translucent.

Measurements. See Table 1.

Variation. Several age-independent quantitative characters are recorded for the immature paratypes. Paratype male: (1) PTC 8/8; (2) ID 7/7, OD 14/14, MD 89/89, IAD 53/51; (3) PVTC 8/8. Paratype female: (1) PTC 7/7; (2) ID 5/6, OD 13/14, MD 83/86, IAD 54/55; (3) PVTC 8/8. It is noteworthy that pectinal teeth were not brownish but rather light yellow in the two immature paratypes, manifesting a marked color contrast against the dark brown pectinal lamellae. We are, however, uncertain if this indicates an anomaly in the holotype or a presence of ontogenetic variation. Concerning the unequivocal ontogenetic variation, the immature male possessed a proportionally shorter pedipalp with respect to the carapace length (pedipalp length to carapace length ratio ca. 4.18 in paratype male and ca. 4.99 in holotype male). The paratype female was not conspicuously different from the paratype male, except for the absence of genital papillae and a pair of smaller pectines with lower PTC, both ontogenetically invariant (sexual dimorphism). The shape of carapacial anteromedian notch and ocular islet was not sexually dimorphic. Proximal lobe of pedipalp movable finger was vestigial in both paratypes.

Affinities. *S. deshpandei* **sp**. **n**. can be confidently distinguished from its two congeneric geographic neighbors based on adult males. From *S. kamengensis* (Bastawade, 2006), it differs as follows: **(1)** pedipalp chela more slender (Fig. 13 vs. Kovařík et al., 2020: fig. 277); **(2)** movable finger with stronger proximal lobe and corresponding notch on fixed finger (Fig. 14 vs. Kovařík et al., 2020: fig. 278); **(3)** ID 5–7 (vs. 5), MD > 82 (vs. 80); **(4)** Eb_3 position type B (vs. A). From *S. novaki*, it differs as follows: **(1)** pedipalp much more slender (Fig. 13 vs. Kovařík, 2005: fig. 15); **(2)** PVTC 7–8 (vs. 8–9) ; **(3)** ID 5–7 (vs. 4), OD 13–14 (vs. 11–13), MD > 82 (vs. 70); **(4)** Eb_3 position type B (vs. A). Considering the known dispersal ability of several species in this genus (Kovařík et al., 2020: fig. 799), we further compared *S. deshpandei* **sp**. **n**. with four other congeners with elongated chelae in nearby regions where it can be readily distinguished from three of those species. From *S. asthenurus* Pocock, 1900, it differs as follows: **(1)** dorsal marginal carina of chela not curved (Fig. 13 vs. Kovařík et al., 2020: fig. 271); **(2)** PVTC 7–8 (vs. 8–9); **(3)** ID 5–7 (vs. 4–5), OD 13–14 (vs. 10–12), MD > 82 (vs. 75); **(4)** Eb_3 position type B (vs. A). From *S. bhutanensis*, it differs as follows: **(1)** pedipalp much less slender (Fig. 13 vs. Lv & Di, 2022a: fig. 1); **(2)** pectines dark brown (vs. yellow; Fig. 9 vs. Lv & Di, 2022a: fig. 13); **(3)** Eb_3 position type B (vs. A). From *S. lii* (Di & Qiao, 2020), it differs as follows: **(1)** pedipalp chela more slender (Fig. 13 vs. Di & Qiao, 2020: fig. 1); **(2)** venter and telson not bright yellow (Figs. 2, 29 vs. Di & Qiao, 2020: figs. 2, 15); **(3)** different pectinal morphology with higher PTC (8 vs. 5–6 in males; Fig. 9 vs. Di & Qiao, 2020: fig. 9); **(4)** Eb_3 position type B (vs. A).

S. deshpandei **sp**. **n**. is undoubtedly most associated with *S. longimanus* Pocock, 1893 from India which warrants particular focus. A photograph depicting the external view of the chela of an adult male in Kovařík et al. (2020: fig. 282) implies that the proximal lobe on movable finger is somewhat weaker in *S. longimanus*. According to a recent redescription of this species based on 54 specimens by Malsawmdawngliana et al. (2022), it is also revealed that pectines are consistently light yellow in *S. longimanus* but dark brown in *S. deshpandei* **sp**. **n**. (Fig. 8; but see above for the note on immature specimens). Based on data from both Kovařík et al. (2020: 128) and Malsawmdawngliana et al. (2022: 6), the male *S. longimanus* is characterized as follows: **(1)** PTC: 6/7 (*n* = 1), 7/7 (*n* = 1),

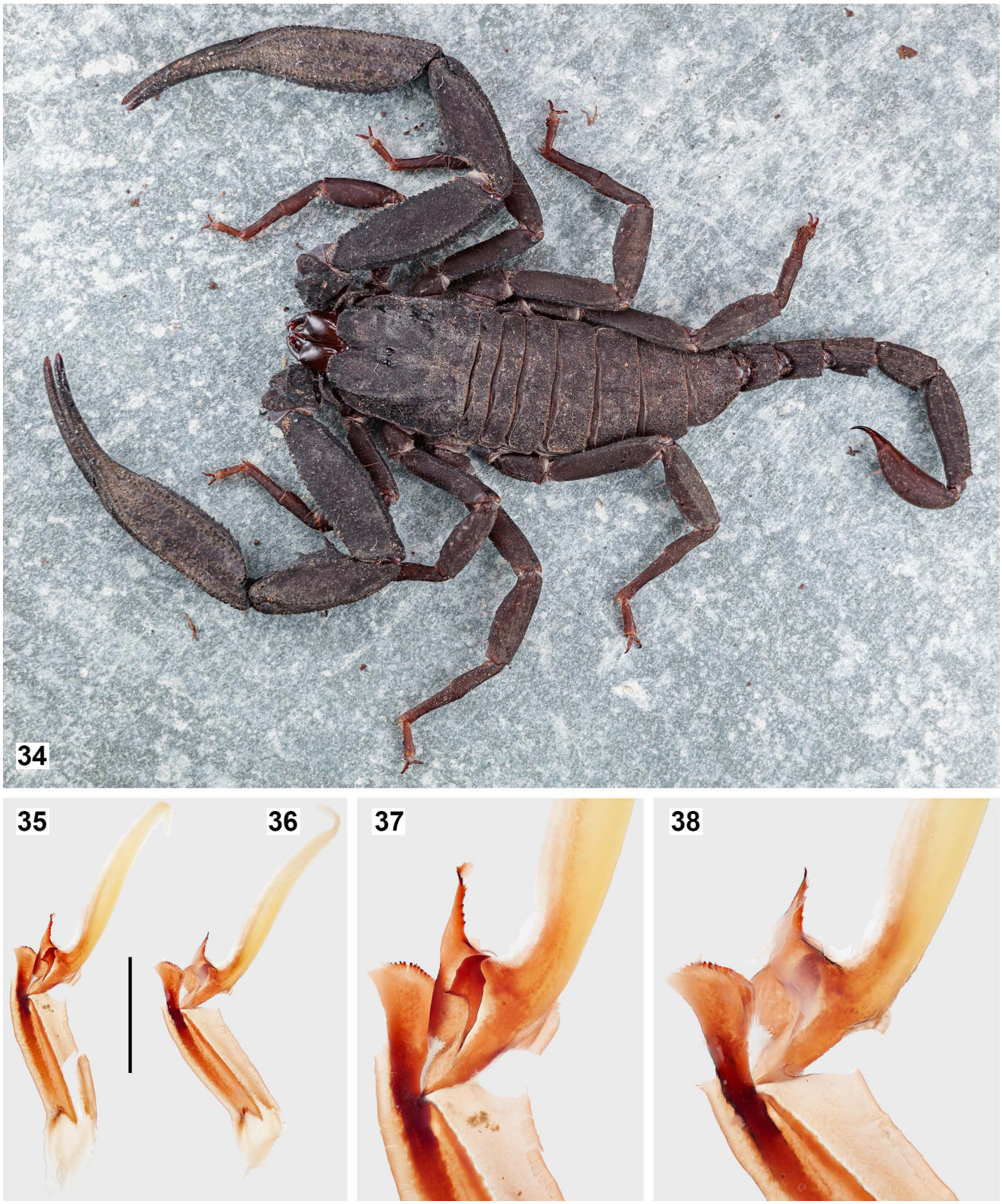

Figures 34–38: *Scorpiops deshpandei* **sp**. **n**., holotype male and hemispermatophore. **Figure 34**. Holotype male in vivo habitus under captive condition. **Figures 35–38**. Paired hemispermatophores in convex (35) and concave (36) views, capsules in convex (37) and concave (38) views. Scale bar = 2 mm (Figs. 35–36).

8/7 (*n* = 1), 9/8 (*n* = 2); **(2)** PVTC: 9–11 (usually 10–11); **(3)** PETC: 18–19; **(4)** IAD: 50–60; **(5)** MD: 80; **(6)** ID: 5–6; **(7)** OD: 13–14; **(8)** Eb_3 position type A. While *S. deshpandei* **sp. n.** falls into the variation range of character 1, being identical on character 7, and overlapped in characters 3, 4 and 6 of *S. longimanus*, the discordance in PVTC (7–8), MD count (> 82) and Eb_3 position (type B), allows the differentiation. More importantly, our molecular analysis has further corroborated the status of this species as distinct from *S. longimanus* (Table 3). Collectively, *S. deshpandei* **sp. n.** is notably distinguished by its consistent type B Eb_3 position across all type specimens, a feature in contrast to the type A position observed in all its geographical neighbors possessing elongated pedipalp chelae. Specifically, in *S. deshpandei* **sp. n.**, *Dt* is positioned centrally to distally along the digital carina within the manus, differing from its somewhat proximal location in other species.

It is also appealing to observe a case of regeneration in the holotype male. The fourth right leg experienced loss of telotarsus and partial loss of basitarsus, and ungues and dactyl were regenerated at the extremity of the truncated basitarsus, alongside an increase of setae (Fig. 127). More intriguingly, rows of spinules and ventral vertices of lateroapical margin (= "laterodistal lobes" in Prendini, 2000: 59) typically present on the ventrodistal surface of telotarsus developed on this segment. Axial rows of spinules are absent from the normal 4th basitarsus, while distal marginal spinules may present (Fig. 33). However, those structures on the regenerated segment were even denser than the normal telotarsi. The regeneration and proliferation of those structures may indicate a morphological compensation for the truncated leg to preserve its locomotive function. It is noteworthy that postnatal regeneration after physical damage does not fall under the category of teratology. Teratology is the study of congenital malformations and abnormalities that arise from exposure to teratogens—agents that cause disruptions during embryonic or fetal development. These teratogens can include chemicals, drugs, infections, and environmental factors that interfere with normal developmental processes. In contrast, postnatal regeneration refers to the body's ability to repair and regenerate tissues after birth in response to injury or damage, and does not involve the congenital origins or prenatal developmental disruptions.

Behavioral notes. The holotype of *S. deshpandei* **sp. n.** occasionally exhibited a cataleptic response, particularly after falling to the ground (cf. Tang, 2023: fig. 64). Upon the introduction of tactile stimulus through the touch of a finger, it may either dart for a short distance or remain motionless. However, this specimen displayed notable activity and agility, exhibiting aggression towards perceived threats. An inadvertent sting from this individual on the ventral surface of the index finger led to an immediate pricking sensation, followed by mild itching. However, the unpleasant sensation dissipated shortly after, giving way to moderate swelling.

Distribution. Known only from the type locality.

Scorpiops kovariki sp. n.

(Figures 39–72; Tables 1–2)

http://zoobank.org/urn:lsid:zoobank.org:act:AC035EC1-C699-4C7E-B78D-90D93E591779

Type locality and type depository. **CHINA**, ***Tibet Autonomous Region***, Nyingchi (or Linzhi, Nyingtri) prefecture-level City, Zayü (or Chayu, Zayul) County, 28°33'27.2"N 98°17'36.5"E (28.5575607°N 98.29347779°E), 2492 m a. s. l.; VT.

Type material. **CHINA**, ***Tibet Autonomous Region***, Nyingchi City, Zayü County, 28°33'27.2"N 98°17'36.5"E, 2492 m a. s. l., 15 July 2023, 1♀ (holotype), leg. Tongtong.

Etymology. The specific epithet is a patronym in honor of Czech scorpiologist František Kovařík, a major contributor to the taxonomy of Scorpiopidae, who has also been supporting the first author in her past publications. The nexus between the concrete species and and its nomenclature was established based on its evident resemblance to the congener described by F. Kovařík, *S. jendeki*. Chinese equivalent: 寇氏类蝎 (roughly as "Kovařík's resemblant scorpion" in English; see Tang (2022a) for the rules of designation).

Diagnosis (♀). Total length ca. 33 mm for female. Base color uniformly brownish red to blackish brown; chela with fingers and carinae blackish and manus reddish, telson brownish red, genital plate light brown, pectines light yellow. Cuticular surface (somatic) matte and sparsely but coarsely granular; pedipalp chela manus lustrous. Carapace with anteromedian notch semicircular; ocular tubercle distinct within ocular islet, elliptical in profile; ocular subislets weakly granular and planar; interocular sulcus absent; superciliary carinae smooth. Cheliceral fixed finger with basal and median denticles forming into a bicuspid trunk. PTC 4 in female; fulcra absent; pectines with two marginal and one middle lamellae present (P3); sternites III–VI lustrous, VII granular with four distinct carinae. Pedipalp patella with weak prolateral apophysis; 16–17 external and 5–6 ventral trichobothria. Chela with 4 *V* series trichobothria; Eb_3 located in proximal half of manus between *Dt* and *Db* (type D); Ch-L/W ca. 2.4 in female. Dentate margin of movable fingers not undulate in female, with 9–10 OD, 49–51 MD, 6–7 IAD and 6 ID. Telotarsi of leg I–VI with ca. 6–12 stout median ventral spinules nearly in a single row. Metasoma I–V with 10-8-8-8-7 carinae. Telson moderately short and moderately bulbous, densely covered with fine granules; T-L/D ca. 3.05 in female; annular ring developed.

Description (♀).Overall habitus (Figs. 39–40), prosoma, mesosoma, metasoma and telson, chelicera and legs were photographed under white light. Additional UV fluorescence imaging was applied for prosoma and mesosoma.

Prosoma and mesosoma (Figs. 41–50, 62–63). *Prosoma*: Carapace with 3 pairs of lateral ocelli (two larger, one

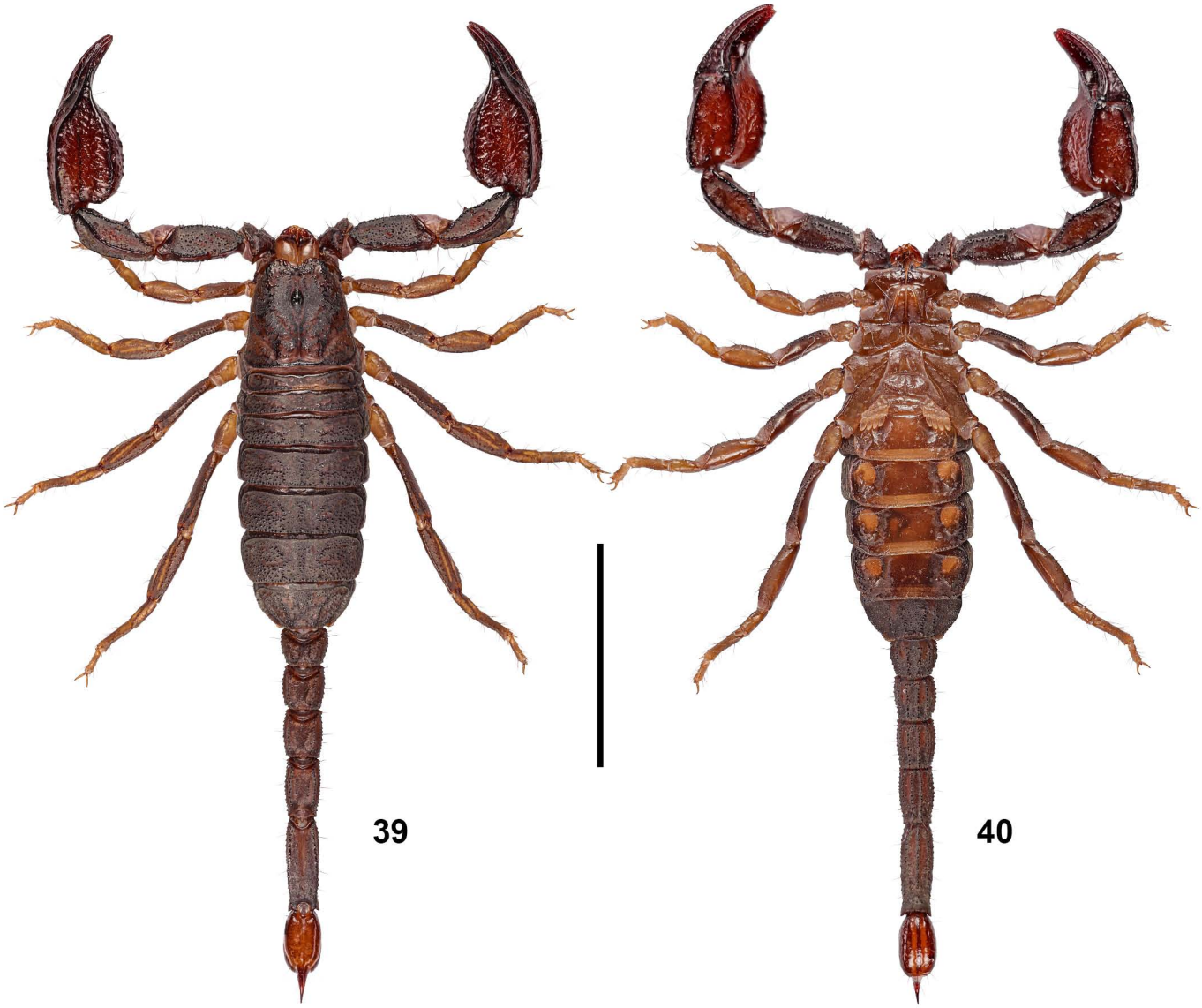

Figures 39–40. *Scorpiops kovariki* **sp. n.**, holotype female, habitus in dorsal (39) and ventral (40) views, under white light. Scale bar = 10 mm.

smaller); median ocular tubercle distinct within ocular islet, elliptical in profile; subislets weakly granular, approximately planar; interocular sulcus absent; superciliary carinae smooth. Dorsomedian part of the carapace (ca. 1/2 of total area) planar, with anterolateral boundaries demarcated by coarse granules; lateral surfaces slanting downwards. Entire carapace moderately covered with fine to median-sized granules, weakly lustrous at non-granular regions; larger and somewhat interfused granules concentrated anteriorly at edges flanking anteromedian sulcus, and above and posterior to lateral ocelli; distinct carinae absent. Anterior margin of carapace with a shallow, semicircular median notch leading to a shallow, smooth anteromedian sulcus; circumocular and posteromedian sulci smooth and matte; lateral surfaces with a pair of indistinct central lateral sulci and prominent posterior lateral sulci, both smooth and matte; posterior marginal sulcus deep. Chelicerae with dorsal surface smooth and ventral surface densely setose on 2/3 area; all denticles of cheliceral fingers relatively blunt but might had been caused by abrasion; basal and median denticles on fixed finger conjoined on a common trunk. *Mesosoma*: All tergites (except for pretergites which are moderately lustrous) covered by a layer of matte, greyish mask, contrasting with the smooth granules that reflect the base color; all tergites covered with moderate to large, somewhat flattened granules, becoming larger closer to posterior margins, with one distinct median carina (less prominent on I–II while concealed by random granules on VII). Sternites III–IV highly lustrous, with sparse macrosetae and fluorescent microsetae as well as two axisymmetric, curved furrows; sternite VII strongly granulated with four granular carinae; respiratory spiracles oval. Genital operculum divided into two halves, without genital papillae at the base. Pectines with two marginal and one middle lamellae present, distal furrow on the right pectine not fully delineated; pectine teeth number 4/4; area of peg sensilla concentrated along the external edge of each pectinal tooth, minute in size; fulcra absent; fluorescent microsetae present.

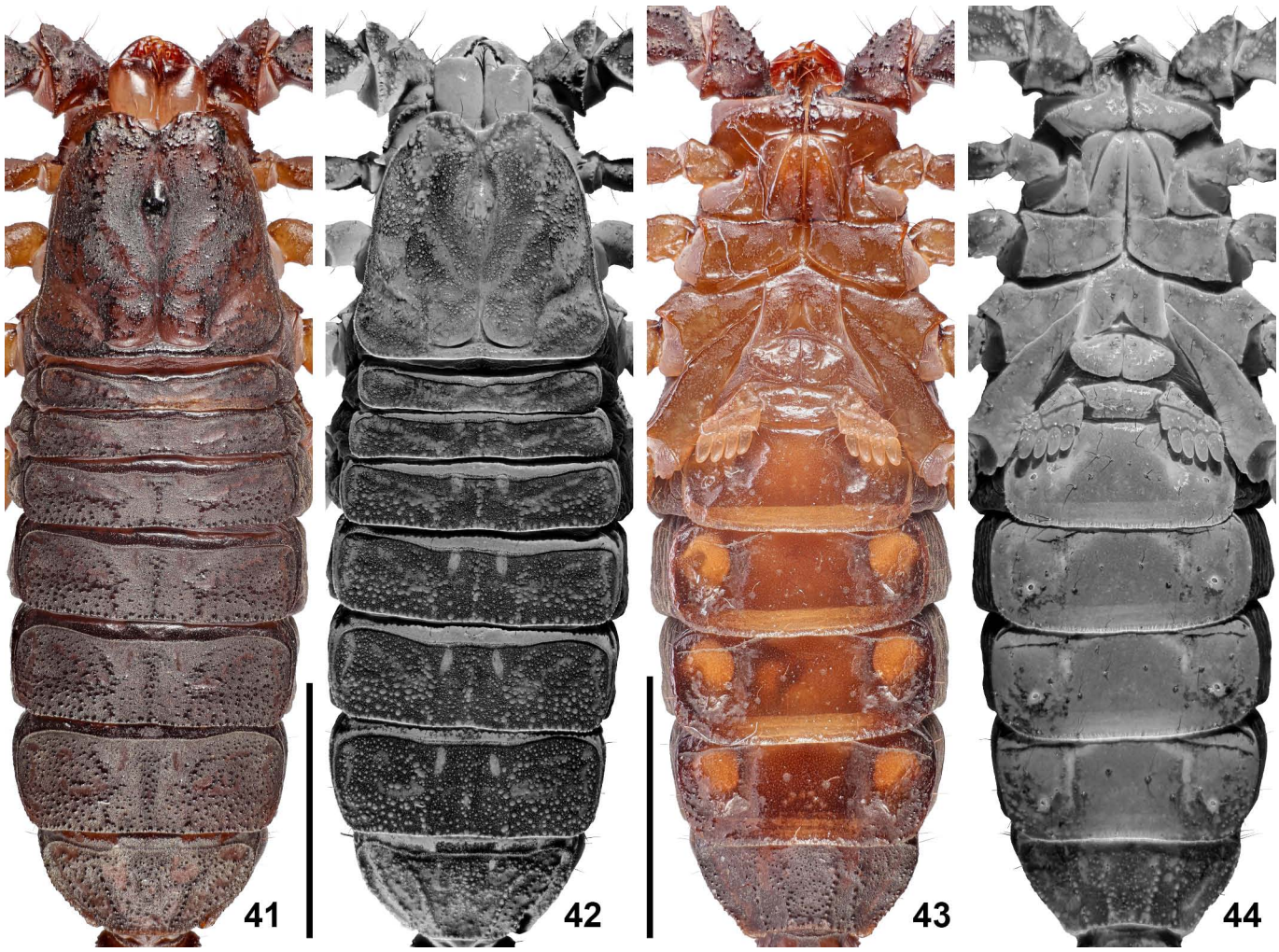

Figures 41–44: *Scorpiops kovariki* **sp. n.**, holotype female, prosoma and mesosoma. **Figures 41–42**. In dorsal view, under white (741) and UV (42) light. **Figures 43–44**. In ventral view, under white (43) and UV (44) light. Scale bar = 5 mm (Figs. 41, 43).

Metasoma and telson (Figs. 64–67). Metasoma sparsely hirsute and weakly granulated; carinae formed by larger granules. Metasoma I with 10 carinae, II–IV with 8 carinae, and V with 7 carinae; median lateral carinae of metasoma II–IV decomposed into random granules and do not form distinct carinae; all carinae serrated, especially the ventrolateral and ventromedian carinae on metasoma V. Anal arch armed with sharp granules. Telson lustrous, very sparsely hirsute, moderately short and bulbous; all surfaces nearly smooth; prominent annular ring developed. Vesicle with lateral surface furnished by one longitudinal sulci close to dorsal surface, and ventral surface with two parallel longitudinal sulci; lateral sulci deeper than ventral sulci. Aculeus smooth, short, weakly curved (tip broken).

Pedipalps (Figs. 51–61). Pedipalps sparsely hirsute, intercarinal surfaces scattered with generally sparse granules and patches of lattice microstructures. Patella with 17/16 external (4/3 *et*, 4 *est*, 2 *em*, 2 *esb*, 5 *eb*; one *esb* closer to *em* series) and 5/6 ventral trichobothria. Chela with 4 *V* series trichobothria; trichobothrium Eb_3 located in proximal half of manus between trichobothria *Dt* and *Db*. Femur with 6 highly granular carinae and a coarsely granulated dorsal surface; retromedian and retroventral carinae incomplete, respectively deconstructed into discrete granules proximally and distally; granules larger on promedian, retrodorsal and proventral carinae. Patella with 5 lustrous, granular or costate carinae and weakly granulated intercarinal surfaces; prodorsal carina granular; proventral carina costate-granular; retrodorsal, retromedian and retroventral carinae costate; granules do form a distinct reticulate configuration on ventral surface; prolateral surface with a triangular apophysis not armed by prominent spiniform granules. Manus sparsely adorned with small to moderate intercarinal granules, which form a reticulate configuration with large hollows on dorsal surface; dorsal secondary carina indicated, gradually diffusing to dispersed granules; subdigital and ventrointernal carinae obsolete; dorsal internal and dorsal marginal carinae evidently separated, with dorsal internal carina indicated by large but flat granules; dorsal marginal, digital, external secondary, ventroexternal, ventromedian and interomedian carinae strongly costate and

Figures 45–50: *Scorpiops kovariki* **sp**. **n**., holotype female, carapace (45, 48), pectines (46, 49), and sternite VII (47, 50). **Figures 45–47**. Under white light. **Figures 48–50**. Under UV light. Scale bar = 2 mm (Figs. 45–46), 1 mm (Fig. 47).

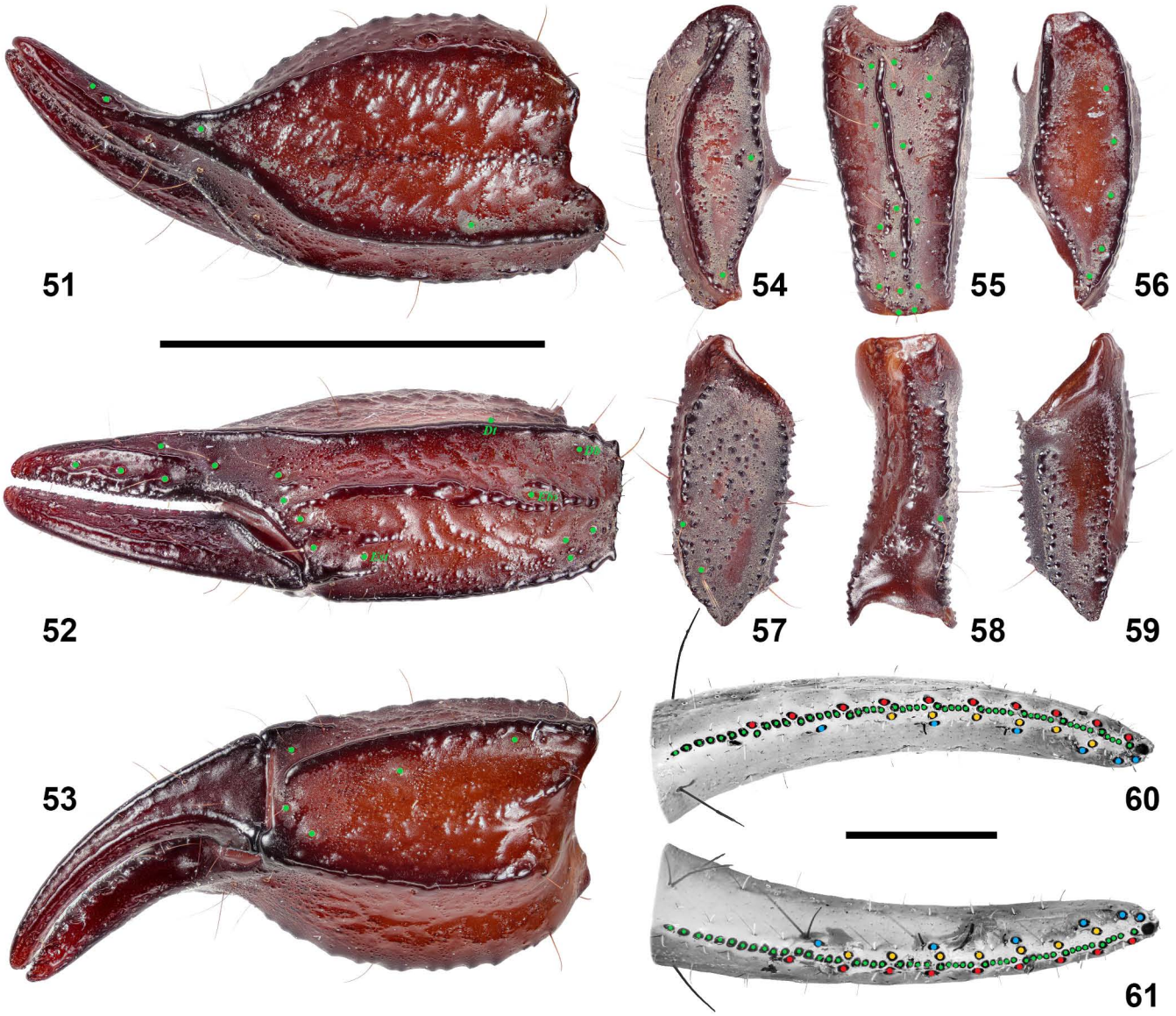

Figures 51–61: *Scorpiops kovariki* **sp**. **n**., holotype female, pedipalp. **Figures 51–59**. Chela in dorsal (51), external (52), and ventral (53) views, patella in dorsal (54), external (55), and ventral (56) views, femur in dorsal (57), external (58), and ventral (59) views under white light. **Figures 60–61**. Left (60) and right (61) movable fingers in dorsal view, under UV light. Scale bar = 5 mm (Figs. 51–59), 1 mm (Figs. 60–61).

lustrous. Dentate margin of movable fingers not undulate (proximal lobe absent), adorned by 10/9 OD, 51/49 MD, 6/7 IAD (same size as OD and ID) and 6/6 ID; IAD series creates an incomplete second row along MD series, paired with OD distally, which divide the entire MD series into several subrows, each ended in a slightly enlarged MD.

Legs (Figs. 68–71). Tibia and tarsomeres of legs with several macrosetae not arranged into bristle combs. Basitarsi of legs I–II with two rows of dense, short spinules, becoming vestigial on legs III and IV; a pair of pedal spurs present on the distal margin of all basitarsi (one lost due to injury on IV). Telotarsi of legs I–IV with a row of short, stout ventromedian spinules (ca. 6–12 in number). Ungues moderately short, stout and curved. Carinae on femur and patella distinct, granular to costate-granular.

Measurements. See Table 1.

Affinities. *S. kovariki* **sp**. **n**. can be confidently differentiated from all its Tibetan congeners, even those dark colored species with stout chelae, including *S. atomatus*, *S. ingens*, *S. langxian* Qi et al., 2005, *S. lourencoi*, *S. margerisonae* and *S. tibetanus*, by a completely different pectine morphology (short and light yellow, comprising only four teeth; Figs. 46, 49), alongside a plethora of other pronounced distinctions. Intriguingly, this species showcases a remarkable resemblance with *S. jendeki* from Yunnan. *S. jendeki* is the most widespread *Scorpiops* species in Yunnan with its northmost occurrence in Gongshan County, Nujiang Lisu Autonomous Prefecture (Tang, 2023: table 2; adjacent with the type locality of *S. kovariki* **sp**. **n**.); recent investigation also revealed its occurrence in Kachang, Yingjiang County (pers. comm., Tongtong). Both species are small in size, with short, robust pedipalps bearing movable fingers devoid of proximal lobes, as well as relatively short

pectines and sparsely granulated tergites. Detailed photographs of *S. jendeki* can be referred from Tang (2023: figs. 97–100, 137, 146, 155, 164, 173–174, 196–199). Cursory examination on the holotype female detected a pair of proportionally small median ocelli and lustrous pedipalp manus and telson in contrast to *S. jendeki*, which led us to suspect its identity. To eliminate the possibility that the glossy appearance of the chela and telson observed in the holotype of *S. kovariki* **sp**. **n**. was not unique to this species, additional specimens of *S. jendeki* previously collected from Yunnan were reexamined (partially listed in Tang, 2023: 2). It was ascertained that, at least on the basis of the 21 specimens examined, *S. jendeki* is not characterized by a smoothness on chelae. Comparative photos of those specimens, with the holotype of *S. kovariki* **sp**. **n**., are included in the supplementary PDF file.

Following a scrutiny upon the holotype of *S. kovariki* **sp**. **n**., several morphological distinctions from *S. jendeki*, confined to the comparison between adult females, are proposed: **(1)** carapacial anteromedian notch proportionally shallow and semicircular (vs. typically deep and dome-shaped in *S. jendeki*; cf. Fig. 48 vs. Tang, 2023: fig. 146); **(2)** ocular islet proportionally longer with respect to the median ocelli but smaller with respect to the carapace, with an elliptical ocular tubercle (vs. shorter and larger with a rounded ocular tubercle in *S. jendeki*; cf. Fig. 48 vs. Tang, 2023: fig. 146); **(3)** relatively small median ocelli with respect to the carapace (cf. Fig. 48 vs. Tang, 2023: fig. 146); **(4)** carapace somewhat more flattened and less triangular (cf. Fig. 48 vs. Tang, 2023: fig. 146); **(5)** pedipalp chela manus lustrous (vs. matte in *S. jendeki*; cf. Figs. 72–73); **(6)** dorsal internal carinae of chela manus with fewer and weaker granules (vs. typically prominent and strongly spiniform in *S. jendeki*; cf. Fig. 51 vs. Tang, 2023: fig. 99); **(7)** region along the dorsal marginal on dorsal surface of manus not adorned by darkened granules (vs. densely adorned by darkened granules in *S. jendeki*; cf. Fig. 51 vs. Tang, 2023: fig. 99); **(8)** dorsal marginal, external secondary and ventromedian carinae of chela manus highly costate (vs. costate-granular to granular in *S. jendeki*; cf. Figs. 51–52 vs. Tang, 2023: figs. 99–100); **(9)** retrodorsal carinae of pedipalp patella costate (vs. granular to costate-granular in *S. jendeki*; cf. Fig. 54 vs. Tang, 2023: fig. 174); **(10)** mesosoma with a distinct median carina and denser and coarser granules exhibiting stronger between-granule size contrast (vs. median carina less discernable, with granules being sparse and ambiguous; cf. Fig 42 vs. Tang, 2023: fig. 164, and Figs. 72–73); **(11)** telson slightly more lustrous (cf. Figs. 72–73); **(12)** pectines with less dense fluorescent microsetae (cf. Fig. 49 vs. Tang, 2023: fig. 199).

With reference to Kovařík et al. (2020: 129, table 9), the only reliable quantitative disparity between the two species appears to lie in the count of IAD (6–7 in *S. kovariki* **sp**. **n**. vs. 10 in *S. jendeki*). 18 specimens of *S. jendeki* were counted for their finger denticles, with two of which represented by a single finger respectively (number of fingers n = 34, including the one examined in Kovařík et al. (2020)). While their illustration indeed displayed an evident count of 10 IAD (Kovařík et al., 2020: 18, fig. 115), a noticeable level of intricacy was observed in the materials examined herein. Specifically, additional denticles may be present at the proximo-internal side flanking the main MD series. They represent a category of complex denticles that had been considered as a part of the MD series in Tang (2022b, 2023). There may be no explicit hiatus between those denticles and the preceding definitive IAD as shown in Kovařík et al. (2020). Unbiasedly incorporating all these denticles into the IAD series would result in a considerable degree of variability in the count of IAD for *S. jendeki* (ca. 9–18, mean ± standard deviation = 13.35±1.98). On the other hand, a biased count rendered a total range of ca. 7–10 (mean ± standard deviation = 8.44±0.66), with the determination based on the subjectively perceived interdental distance and whether the pertinent denticle is paired with an OD on the opposing side. Given the potential ambiguity in distinguishing between IAD and MD, their sum (mean ± standard deviation = 65.74±2.73) was therefore calculated for comparison with that of *S. kovariki* **sp**. **n**. The examined 34 movable fingers of *S. jendeki* yielded a biased MD (defined as sum minus biased IAD) of 57.29±2.74 (mean ± standard deviation; range 50–62). As an additional reference, the IAD and MD counts of *S. kovariki* **sp**. **n**. was further compared the biased IAD and MD counts of *S. jendeki*. A simple linear regression test was performed to detect the possible correlation between left and right finger denticle counts of the 16 examined *S. jendeki* specimens: (1) sum comparison, R^2 = 0.3655 (Pearson's r = 0.6046), p = 0.01311; (2) biased IAD comparison, R^2 = 0.04368 (Pearson's r = -0.209), p = 0.4373; (3) biased MD comparison, R^2 = 0.4607 (Pearson's r = 0.6788), p = 0.00384. Since one of the correlations was weak, we first treated these 32 fingers as independent and included the two solitary fingers (hence n = 34 in total). Those data were compared against the data (two fingers) of *S. kovariki* **sp**. **n**., which yielded a statistically significant difference (two-sample Mann-Whitney U test): (1) sum comparison, p = 0.02018; (2) biased IAD comparison, p = 0.01165; (3) biased MD comparison, p = 0.02398. Alternatively, we compared the means between the two species (for *S. jendeki*, the data of two solitary fingers represented their own mean, hence n = 18). Shapiro-Wilk test was first taken to confirm normality in the count of *S. jendeki*: (1) sum data confirmed normal: W = 0.9833, p = 0.9774; (2) biased IAD data confirmed non-normal (symmetrical but leptokurtic): W = 0.8687, p = 0.01696; (3) biased MD data confirmed normal: W = 0.9812, p = 0.9613. Consequently, a one-sample t-test was used for the sum and biased MD comparison, which yielded p-values of 1.088e-14 and 3.197e-10 respectively. An outlier detection for the dataset comprising the mean IAD of all specimens of both species (dataset n = 19) was conducted based on Tukey's fences (k =1.5). Data 6.5 (mean IAD of *S. kovariki* **sp**. **n**.) and 10 (of one *S. jendeki*, which was a solitary value, not a mean) were identified as outliers. When the two solitary counts of two *S. jendeki* were discarded (dataset n = 17), the single outlier was *S. kovariki* **sp**. **n**. If the data of *S. jendeki* (i.e., 16 mean and 2 solitary) were compared with the two raw data of *S. kovariki* **sp**. **n**.

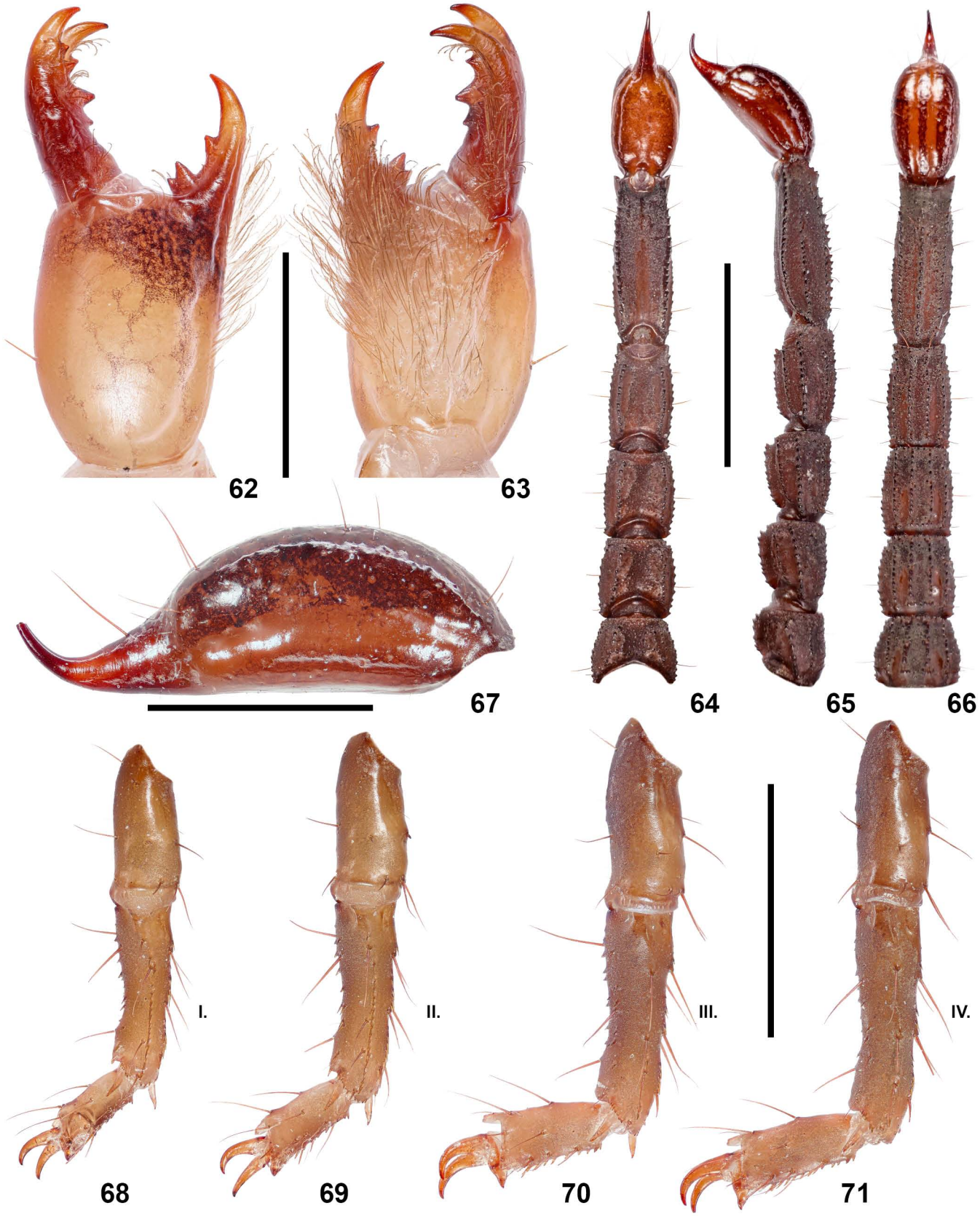

Figures 62–71. *Scorpiops kovariki* **sp. n.**, holotype female, left chelicera in dorsal (62) and ventral (63) views, metasoma and telson in dorsal (64), lateral (65), and ventral (66) views, telson in lateral view (67), left legs I–IV in retrolateral view (68–71), under white light. Scale bar = 500 μm (Figs. 62–63), 5 mm (Figs. 64–66), 2 mm (Figs. 67 horizontal, 68–71 vertical).

Figures 72–73: *Scorpiops* spp. in vivo habitus under captive condition. **Figure 72**. *Scorpiops kovariki* **sp. n.**, holotype female. **Figure 73**. *Scorpiops jendeki* Kovařík, 1994, adult female from Lianghe County (below) and adult male from Kachang, Yingjiang (above) County, Dehong Prefecture.

by two-sample Mann-Whitney U test, a significant *p*-value of 0.02007 was obtained (discarding the two solitary values yielded a lower *p*-value, 0.0192). In all cases, the two counts were found significantly different between the two species. However, these results must be taken with caution as the sample size for *S. kovariki* **sp. n.** is exceedingly small, and our analysis was based on the assumption that the data of that species represent its population mean.

Regrettably, our molecular analysis revealed a low *16S* genetic distance between the two species (0.02, compared to the within-species variation of *S. longimanus*, 0–0.05, as well as the between-species distance of other species; Table 3). However, a low genetic distance is not always a negation of heterospecificity, and phenotypes can exhibit high rates of speciation even when genetic divergence is relatively low between species (Tarvin et al., 2017). Low genetic divergence often favors the assumption that the observed phenotypic difference may be due to intraspecific variation. Empirically, intraspecific phenotypic variation in the genus *Scorpiops* is typically limited to a few diagnostic characters (e.g., total length, trichobothria count, PTC, and ratiometrics of pedipalp chela, finger lobe and telson). Another variable meristic is the pedipalp finger denticle count, where our new species putatively represents an outlier from the variation range of *S. jendeki*. While quantitative characters display obvious variations in this genus, several qualitative characters remain very stable and conserved where their phenotypic plasticity is unprecedent in *Scorpiops* (i.e., no within-species polymorphism), particularly the carination (costate or granular). Those characters were leveraged in the previous species described by the first author, which is now further validated via molecular data (Table 3). Our new species exhibited similar distinctions from its closest congener. As a result, we reckon that the holotype female does not represent a new record of *S. jendeki* in Xizang, but rather a distinct yet closely related species. The most salient characters that distinguish *S. kovariki* **sp. n.** from *S. jendeki* are the lustrous pedipalp chela and costate carination in the former (see supplementary PDF for more photos).

Behavioral notes. The holotype of *S. kovariki* **sp. n.** had given birth to a brood of scorplings, currently reared by the second author. The first author's observation unveiled a temperament characterized by considerable sensitivity, reminiscent of that exhibited by the holotype *S. matthewi* **sp. n.** However, the holotype *S. kovariki* **sp. n.** displayed a more bellicose demeanor, often resorting to attack the perceived predatory stimulus using its pedipalps and telson. In contrast to adult females of *S. jendeki*, where individuals typically adopted a motionless stance, *S. kovariki* **sp. n.** tended to exhibit a preference for a fight-or-flight response, with cataleptic behavior being rarely observed. Such ethological discrepancy might be species-dependent.

Distribution. Known only from the type locality, but might extend to Yunnan Province.

Scorpiops matthewi **sp. n.**

(Figures 74–107; Tables 1–2)

http://zoobank.org/urn:lsid:zoobank.org:act:FA7BDC98-0021-4157-A4AC-0A5BE3405669

Type locality and type depository. **CHINA**, ***Tibet Autonomous Region***, Xigazê (or Rikaze, Shigatse) City, Samzhubzê (or Sangzhuzi, Samzhubzêqü) District, 29°16'26.1"N 88°52'38.9"E (29.27390958°N 88.87748148°E), 3897 m a. s. l.; VT.

Type material. **CHINA**, ***Tibet Autonomous Region***, Xigazê City, Samzhubzê District, 29°16'26.1"N 88°52'38.9"E, 3897 m a. s. l., 21 July 2023, 1♀ (holotype), 2♀ (paratypes) VT, 1♀ (paratype), FKCP, leg. Tongtong.

Etymology. The specific epithet is a patronym in honor of the American scorpiologist Matthew R. Graham (Eastern Connecticut State University, Willimantic, Connecticut, USA), who kindly helped the first author in finishing the important revision of Xinjiang *Olivierus* (Tang et al., 2024), for his significant contribution to the phylogenetic taxonomy of scorpions. Chinese equivalent: 迈氏类蝎 (roughly as "Matthew's resemblant scorpion" in English; see Tang (2022a) for the rules of designation).

Diagnosis. (♀) Total length ca. 60 mm for fmale holotype. Base color uniformly brownish red to blackish brown; chela with fingers and carinae blackish and manus reddish, telson brownish yellow, genital plate and pectines light yellow with pectinal teeth brownish. Cuticular surface irregularly lustrous and finely granular. Carapace with anteromedian notch dome-shaped; ocular tubercle distinct within ocular islet, elliptical in profile; ocular subislets weakly granular and planar; interocular sulcus weak; superciliary carinae smooth. Cheliceral fixed finger with basal and median denticles not forming into a bicuspid trunk. PTC 4–5 in female; pectines form one compact unit with an incomplete furrow between areas where marginal and middle lamellae are usually delimited (P1); fulcra present but weak; sternites III–VI lustrous, VII granular with four distinct carinae. Pedipalp patella with weak prolateral apophysis; 17 (or 15) external and 6–7 ventral trichobothria in fmale. Chela with 4 *V* series trichobothria; Eb_3 located in proximal half of manus between *Dt* and *Db* (type D); Ch-L/W ca. 2.78 in female holotype manus with external secondary carina strongly developed and costate. Dentate margin of movable fingers weakly to moderately undulate in female, with 8–9 OD, 59–71 MD, 20–31 IAD and 6 ID. Telotarsi of leg I–VI with 8–10 stout median ventral spinules nearly in a single row. Metasoma I–V with 10-8-8-8-7 carinae. Telson relatively short and highly bulbous, densely covered with fine granules; T-L/D ca. 2.54 in holotype female; annular ring developed.

Description (♀ holotype).Overall habitus (Figs. 74–75), prosoma, mesosoma, metasoma and telson, chelicera and

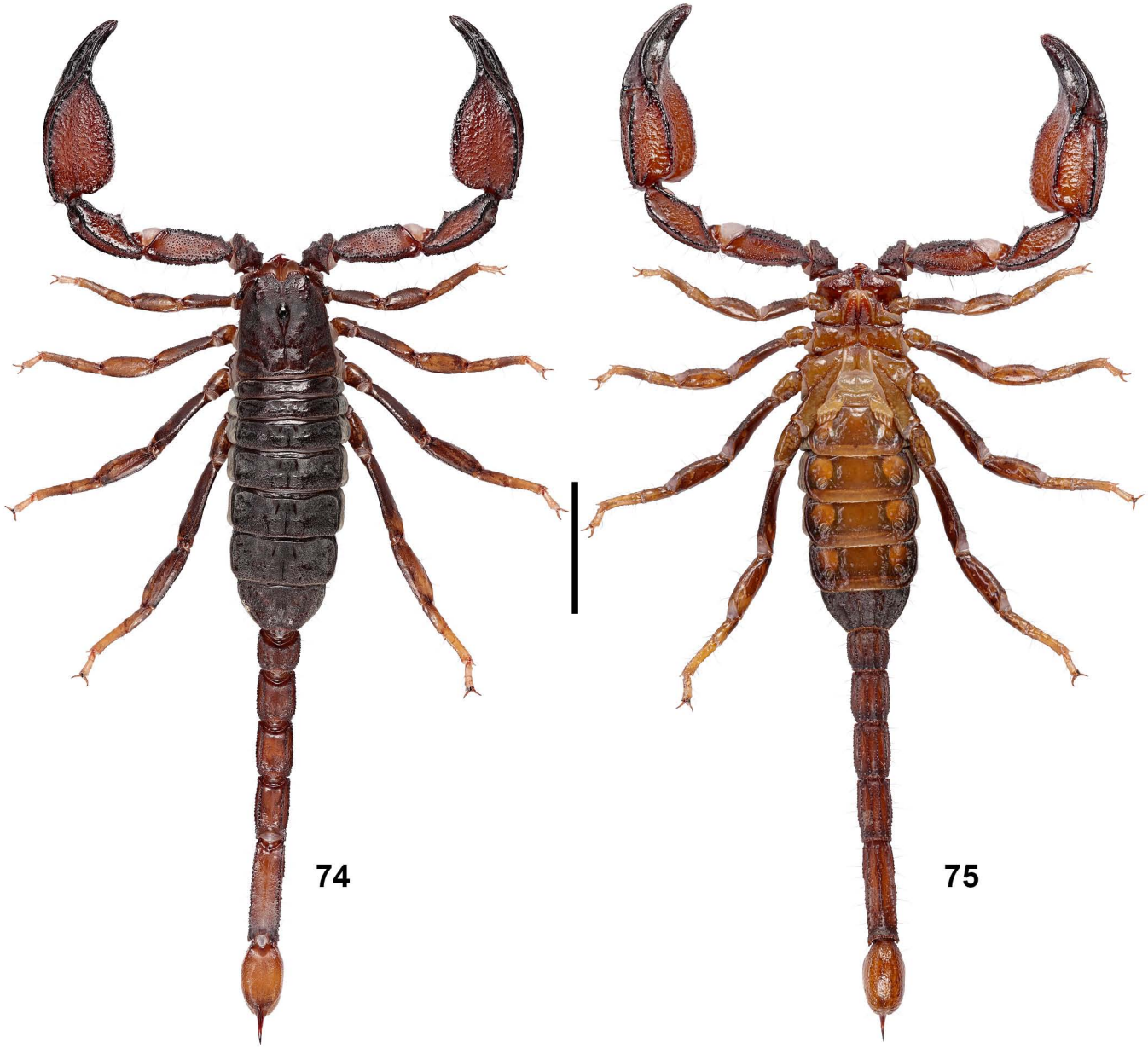

Figures 74–75. *Scorpiops matthewi* **sp. n.**, holotype female, habitus in dorsal (74) and ventral (75) views, under white light. Scale bar = 10 mm.

legs were photographed under white light. Additional UV fluorescence imaging was applied for prosoma and mesosoma. Sparkles presented on the cuticle (prominent in UV photos) due to its highly lustrous texture.

Prosoma and mesosoma (Figs. 76–85, 97–98). *Prosoma*: Carapace with 3 pairs of lateral ocelli (two larger, one smaller); median ocular tubercle distinct within ocular islet, elliptical in profile; subislets finely granular, approximately planar; interocular sulcus weak; superciliary carinae smooth. Dorsomedian part of the carapace (ca. 1/2 of total area) planar, without obvious boundary; lateral surfaces slanting downwards. Entire carapace densely covered with fine granules, but highly lustrous at non-granular regions; larger granules concentrated anteriorly at edges flanking anteromedian sulcus, and above and posterior to lateral ocelli; distinct carinae absent. Anterior margin of carapace with a prominent, dome-shaped median notch leading to a shallow, finely granulated anteromedian sulcus; circumocular and posteromedian sulci lustrous; lateral surfaces with a pair of shallow central lateral sulci and prominent posterior lateral sulci, both lustrous; posterior marginal sulcus deep. Chelicerae with dorsal surface smooth and ventral surface moderately setose along the fixed finger; all denticles of cheliceral fingers relatively blunt but might had been caused by abrasion; basal and median denticles on fixed finger not strongly conjoined on a common trunk. *Mesosoma*: Tergites I–III highly lustrous, VII coarsely granulated and pentacarinate; all tergites covered with small to moderate, somewhat flattened granules, becoming larger closer to posterior margins, with one very weak median carina indicated (more prominent on VI–IV while concealed

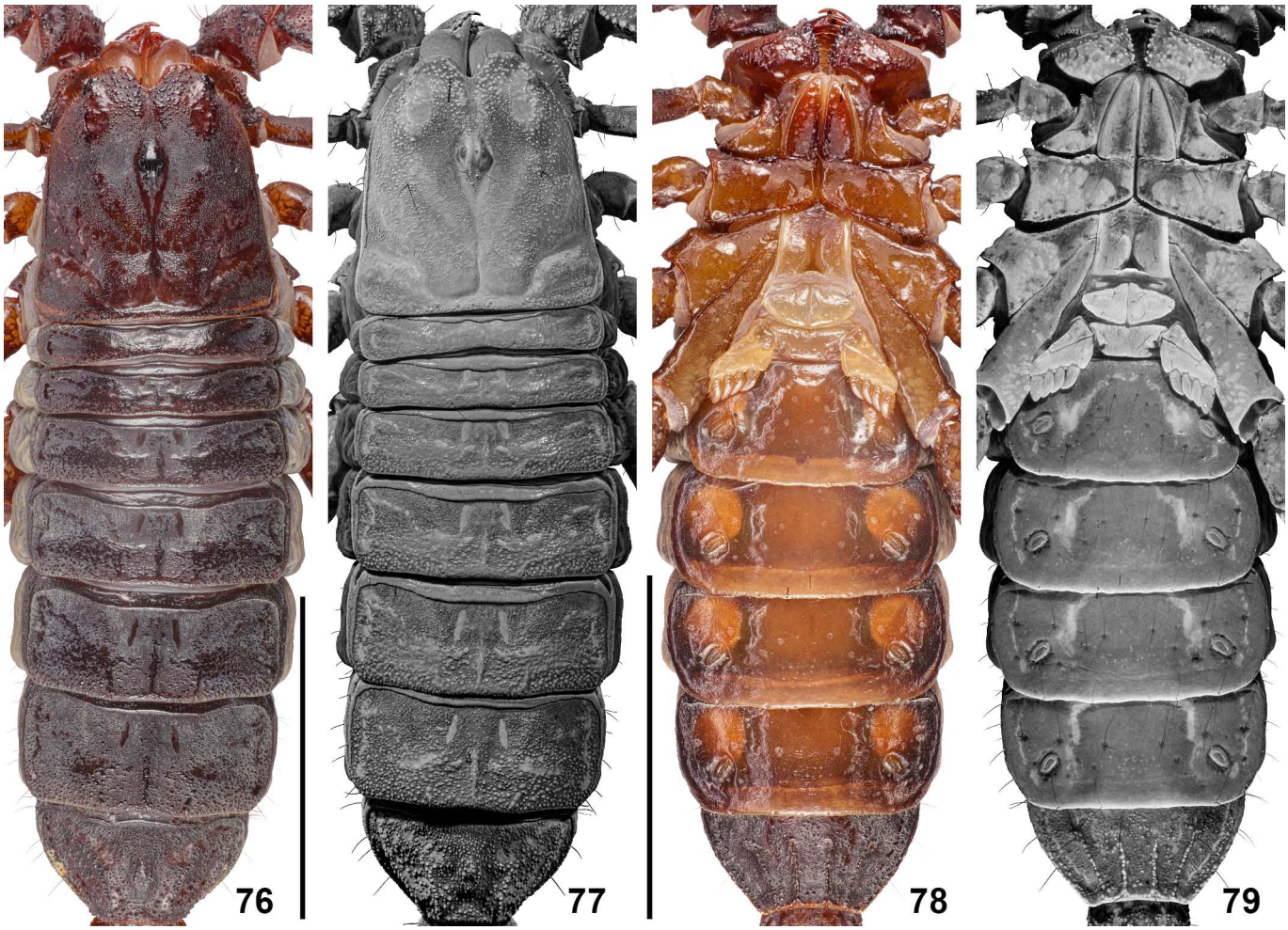

Figures 76–79: *Scorpiops matthewi* **sp. n.**, holotype female, prosoma and mesosoma. **Figures 76–77**. In dorsal view, under white (76) and UV (77) light. **Figures 78–79**. In ventral view, under white (78) and UV (79) light. Scale bar = 10 mm (Figs. 76, 78).

by random granules on VII). Sternites III–IV highly lustrous, with sparse macrosetae and fluorescent microsetae as well as two axisymmetric, curved furrows; sternite VII strongly granulated with four granular carinae; respiratory spiracles suboval. Genital operculum divided into two halves, without genital papillae at the base. Pectines form one compact unit with incomplete furrow between areas where marginal and middle lamellae are usually delimited; pectine teeth number 7/7; area of peg sensilla concentrated along the external edge of each pectinal tooth; fulcra present but weak; fluorescent microsetae present.

Metasoma and telson (Figs. 99–102). Metasoma sparsely hirsute but densely granulated; carinae formed by larger granules. Metasoma I with 10 carinae, II–IV with 8 carinae, and V with 7 carinae; median lateral carinae of metasoma II–IV decomposed into random granules and do not form distinct carinae; all carinae serrated, especially the ventrolateral and ventromedian carinae on metasoma V. Anal arch armed with sharp granules. Telson lustrous, very sparsely hirsute, proportionally short and very bulbous; dorsal surface adorned by fine granules, other surfaces with denser and larger granules; prominent annular ring developed. Vesicle with lateral surface furnished by one longitudinal sulci close to dorsal surface, and ventral surface with two parallel longitudinal sulci; all four sulci relatively shallow and basically smooth (covered with extremely minute granules). Aculeus smooth, short, weakly curved.

Pedipalps (Figs. 86–96). Pedipalps sparsely hirsute, intercarinal surfaces scattered with small to moderate granules and patches of lattice microstructures. Patella with 17 external (4 *et*, 4 *est*, 2 *em*, 2 *esb*, 5 *eb*; one *esb* closer to *em* series) and 7 ventral trichobothria. Chela with 4 *V* series trichobothria; trichobothrium Eb_3 located in proximal half of manus between trichobothria *Dt* and *Db*. Femur with 6 highly granular carinae and a densely granulated dorsal surface; retromedian and retroventral carinae incomplete, respectively deconstructed into discrete granules proximally and distally; granules larger on promedian, retrodorsal and proventral carinae. Patella with 5 lustrous, granular or costate carinae and an unevenly granulated dorsal surface; prodorsal carina granular; retrodorsal and proventral carinae costate-granular; retromedian and retroventral carinae costate; granules form a reticulate configuration on ventral surface; prolateral surface with a triangular apophysis armed with four short spiniform granules. Manus densely adorned with small to moderate intercarinal granules, which form a reticulate configuration on

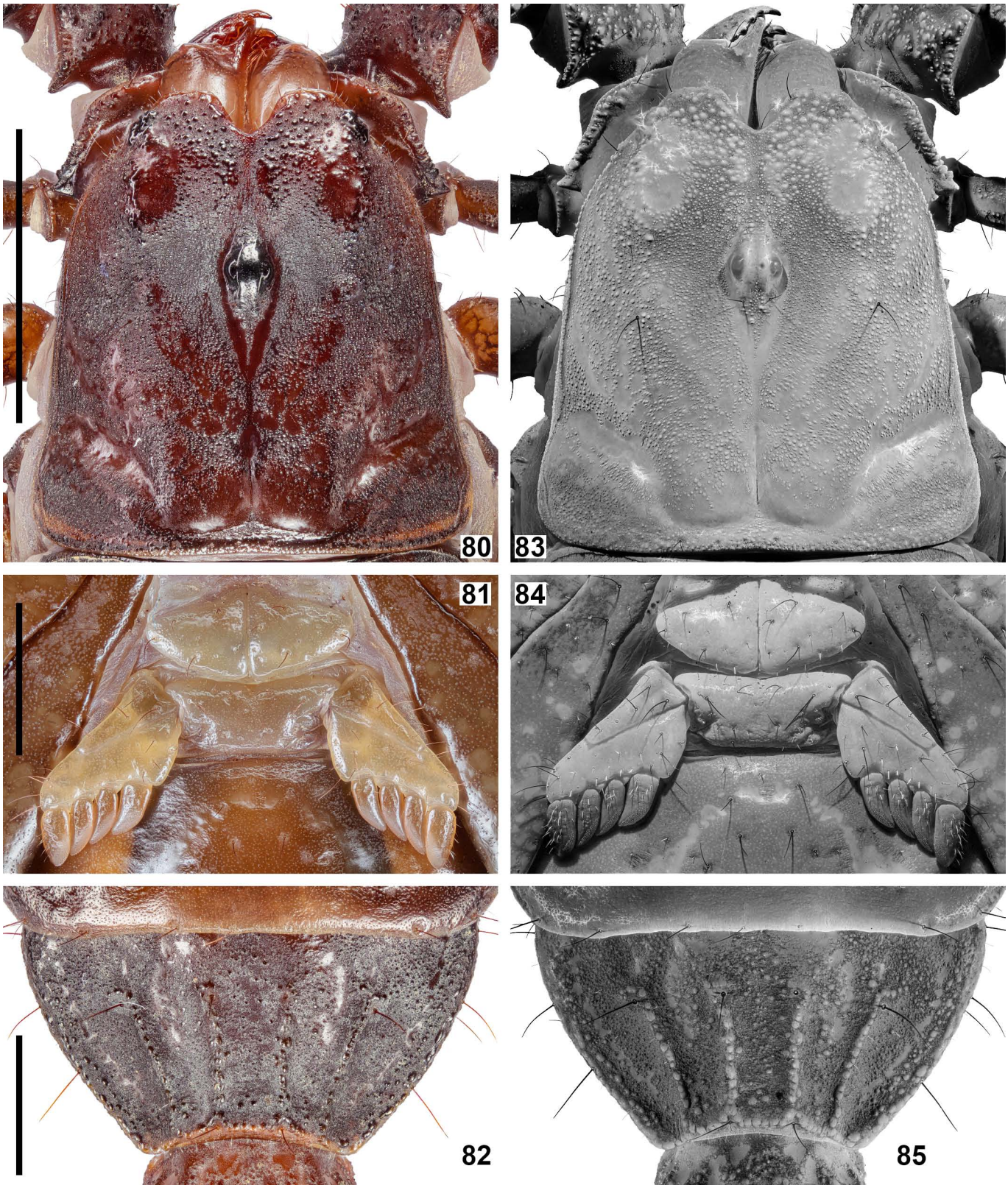

Figures 80–85: *Scorpiops matthewi* **sp. n.**, holotype female, carapace (80, 83), pectines (81, 84), and sternite VII (82, 85). **Figures 80–82**. Under white light. **Figures 83–85**. Under UV light. Scale bar = 5 mm (Fig. 80), 2 mm (Figs. 81–82).

dorsal surface; dorsal secondary, subdigital and ventrointernal carinae obsolete, gradually diffusing to dispersed granules; dorsal internal and dorsal marginal carinae nearly fused, formed by irregular granules; digital, external secondary, ventroexternal, ventromedian and interomedian carinae strongly costate and lustrous. Dentate margin of movable

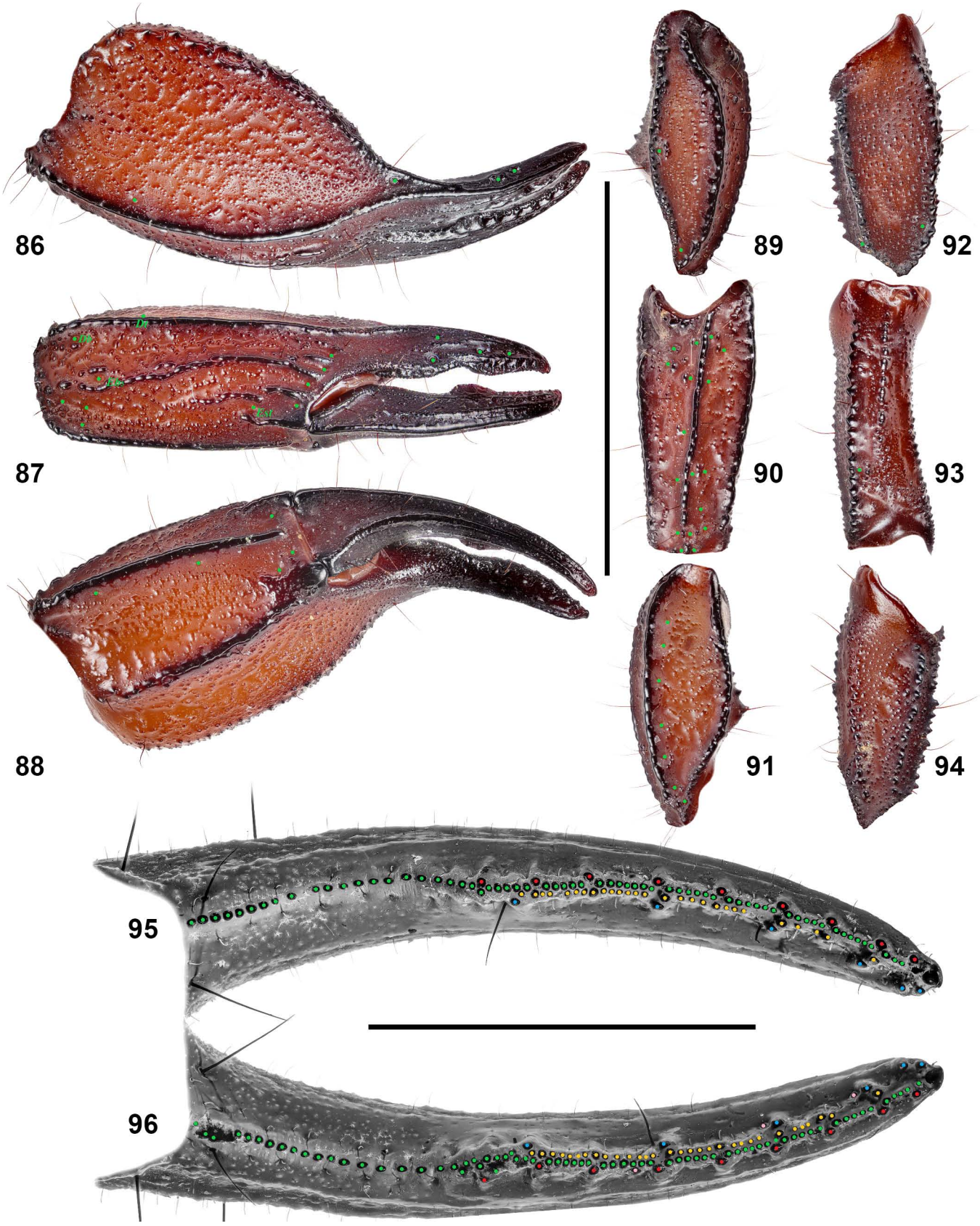

Figures 86–96: *Scorpiops matthewi* **sp**. **n**., holotype female, pedipalp. **Figures 86–94**. Chela in dorsal (86), external (87), and ventral (88) views, patella in dorsal (89), external (90), and ventral (91) views, femur in dorsal (92), external (93), and ventral (94) views under white light. **Figures 95–96**. Left (95) and right (96) movable fingers in dorsal view under UV light. Scale bar = 10 mm (Figs. 86–94), 3 mm (Figs. 95–96).

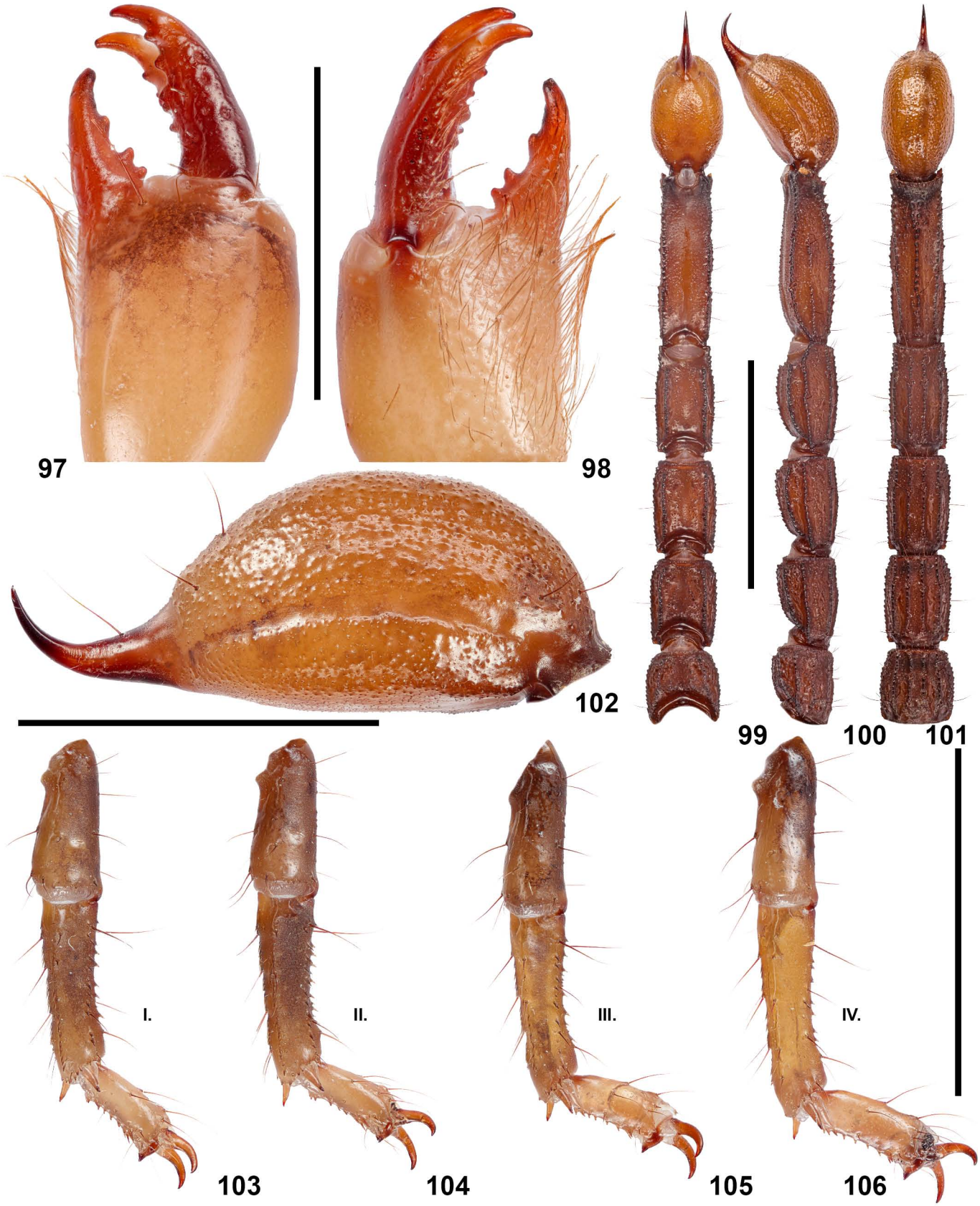

Figures 97–106. *Scorpiops matthewi* **sp. n.**, holotype female, right chelicera in dorsal (97) and ventral (98) views, metasoma and telson in dorsal (99), lateral (100), and ventral (101) views, telson in lateral view (102), right legs I–IV in retrolateral view (103–106), under white light. Scale bar = 2 mm (Figs. 97–98), 10 mm (Figs. 99–101), 5 mm (Figs. 102 horizontal, 103–106 vertical).

Figures 107–108: *Scorpiops* spp. in vivo habitus under captive condition. **Figure 107**. *Scorpiops matthewi* **sp. n.**, holotype female. **Figure 108**. *Scorpiops margerisonae* Kovařík, 2000, subadult (?) female.

fingers moderately undulate (proximal lobe present), adorned by 9/9 OD, ca. 65/71 MD, 27/31 IAD (smaller than MD) and 6/6 ID (3rd and 4th ID on right finger each with one additional denticle, marked in pink; also one additional denticle on the outer side); IAD series creates a second row along MD series, several enlarged IAD may be paired with OD distally, which divide both MD and IAD series into several subrows.

Legs (Figs. 103–106). Tibia and tarsomeres of legs with several macrosetae not arranged into bristle combs. Basitarsi of legs I–II with two rows of dense, short spinules, while one

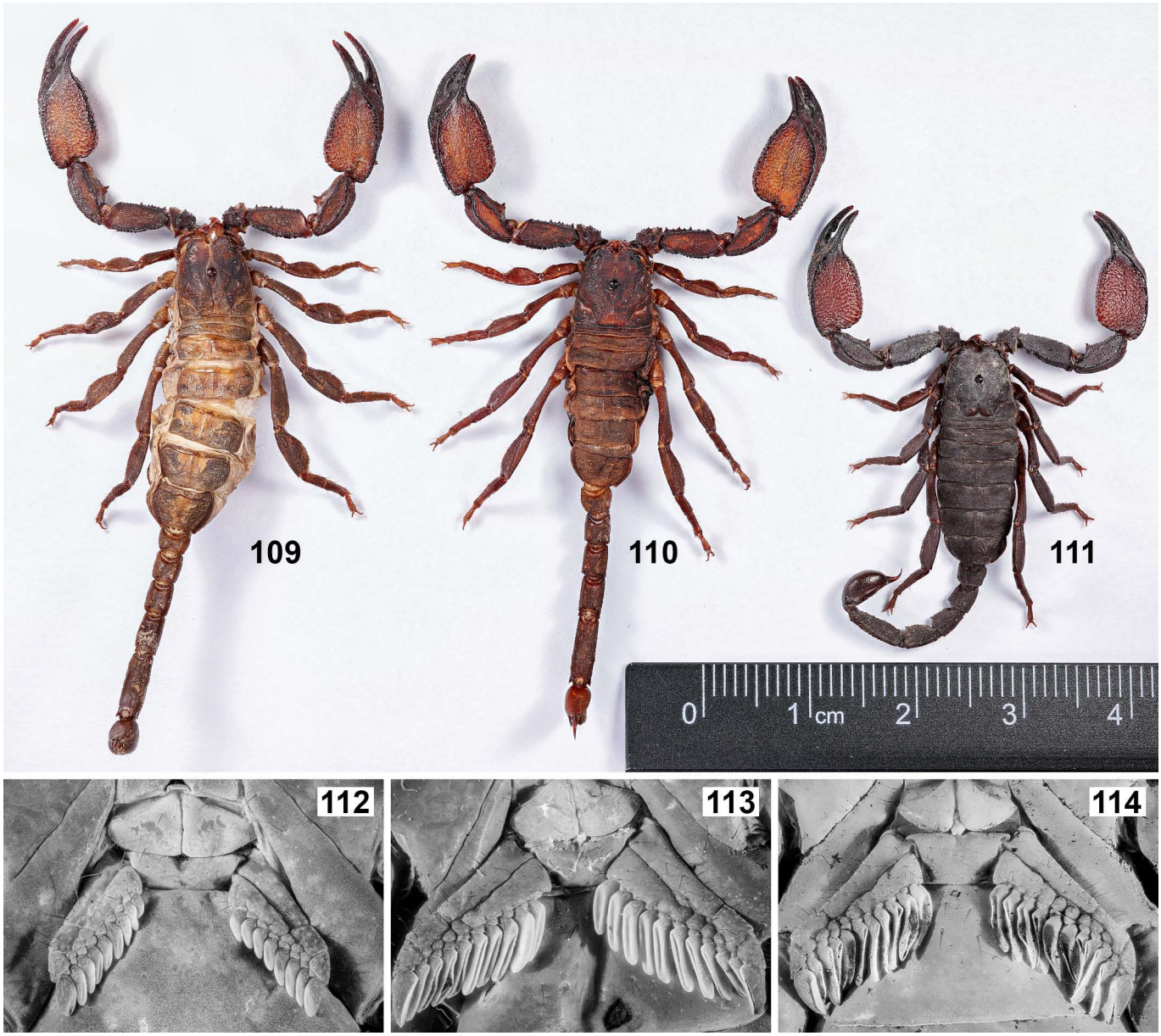

Figures 109–114: Comparison between *Scorpiops wrzecionkoi* Kovařík, 2020 and *S. margerisonae* Kovařík, 2000. **Figures 109–111**. Habitus of female (109) and male (110) *S. wrzecionkoi* and male *S. margerisonae* (111) under white light against an A4 paper background. **Figures 112–114**. Pectines of female (112) and male (113) *S. wrzecionkoi* and male *S. margerisonae* (114) under UV light against black background.

row becomes sparser on leg III and absent on leg IV; a pair of pedal spurs present on the distal margin of all basitarsi. Telotarsi of legs I–IV with a row of short, stout ventromedian spinules (8–10 in number) of which two are always paired on the distal end. Ungues moderately short, stout and curved. Carinae on femur and patella either finely granular or costate. **Measurements**. See Table 1.

Variation. The two paratype females examined by the first author were documented with the following values: **(1)** paratype 1 (finger apically broken, dentition data not included in the diagnosis): PTC 4/4, ID 4/4, OD 9/8, MD 61/67, IAD 18/16, PVTC 7/7, PETC 15(4 *et*, 3 *est*, 1 *em*, 2 *esb*, 5 *eb*)/15(3 *et*, 4 *est*, 2 *em*, 2 *esb*, 4 *eb*); **(2)** paratype 2: PTC 4/4, ID 6/6, OD 8/8, MD 59/61, IAD 23/20, PVTC 6/7, PETC 17(4 *et*, 4 *est*, 2 *em*, 2 *esb*, 5 *eb*)/17(4 *et*, 4 *est*, 2 *em*, 2 *esb*, 5 *eb*). In all examined specimens, the distal *esb* always presented on nearly the same level with the two *em*. Paratype 3 was indirectly examined via the photographs taken by the second author, and its PTC and PVTC were counted as 5/5 and 7/7, respectively. Photographs of the paratypes can be accessed from the supplementary PDF.

Affinities. *S. matthewi* **sp**. **n**. can be confidently differentiated from its two sympatric congeners based on adult females. From *S. tibetanus* (earlier records suggest its presence in this region but further study is required to confirm the identity; Tang, 2023: 48), it differs as follows: **(1)** pedipalp chela

Species	TL	PTC	ID	OD	MD	IAD	PVTC	PETC	Ch-L/W	T-L/D	MF-L	OI	*Eb*$_3$ pos.	P	F
S. asthenurus	35–45	♂ 8–9 ♀ 7–8	4–5	10–12	75	60	8–9	18	♂ 3.2–3.7 ♀ 3.2–3.5	♂ 3.2 ♀ 3.5	♂ **moderate** ♀ weak	OI-2?	A	P2	1
S. atomatus *	35–45	♂ 10–11 ♀ 8–9	5	7–9	58–62	8–9	8–10	17	♂ 2.3 ♀ 2.5	♂ **2.67** ♀ **2.68**	♂ **strong** ♀ **moderate**	OI-1	**D**	**P4**	1
S. bhutanensis **	46–52	♂ 7 ♀ 6–7	-	-	-	-	7–8	17–19	♂ 6.5–7.7 ♀ 3.8	♂ **3.22** ♀ **3.45**	♂ **weak** ♀ **weak**	OI-3	**A**	P3	1
S. deshpandei **sp. n.**	**54** (♂)	♂ **8** ♀ **7**	**5–7**	**13–14**	**83–97**	**51–65**	**7–8**	**17–18(?)**	♂ **4.78** ♀ -	♂ **3.57** ♀ -	♂ **weak** ♀ -	OI-3	**B**	**P4**	**1**
S. ingens	70–76	♂ 7–8 ♀ 6–7	-	-	-	-	6–8	17	♂ 2.3 ♀ 2.5	♂ 2.6–2.7 ♀ 2.6–2.7	♂ **strong** ♀ **weak**	OI-1	D	P3	0
S. kamengensis	42–46	♂ 9 ♀ 4–7	5	12–14	80	60	7–8	18–19	♂ 4 ♀ -	♂ 3.7 ♀ -	♂ **absent** ♀ absent	-	A	P3	1
S. kovariki **sp. n.**	**33** (♀)	♂ - ♀ **4**	**6**	**9–10**	**49–51**	**6–7**	**5–6**	**16–17**	♂ - ♀ **2.41**	♂ - ♀ **3.05**	♂ - ♀ **absent**	OI-1	**D**	**P3**	**0**
S. langxian	52–60	♂ 7–8 ♀ 6	4	8	55	25	6–7	17	♂ 1.9–2.2 ♀ 1.9–2.2	♂ 2.6 ♀ 2.7	♂ **strong** ♀ **weak**	OI-1	D	P3	0
S. leptochirus	40–58	♂ 7–9 ♀ 6–8	4–5	14–15	65	40	6–8	17	♂ 3.8–4.1 ♀ 3.0–3.3	♂ 2.7–2.9 ♀ 2.7–2.9	♂ **absent** ♀ absent	-	D	P1	0
S. lhasa	35–40	♂ *10–11* ♀ *9*	4–5	8–9	55	10	10–11	17	♂ 3.1 ♀ 2.9	♂ 2.8 ♀ 3.0	♂ **moderate** ♀ **weak**	-	E	P4	1
S. lii	37–39	♂ 4–6 ♀ 4–6	-	-	-	-	6–7	17	♂ 3.6 ♀ 3.3–3.4	♂ 2.85 ♀ 3.4–3.5	♂ **strong** ♀ **strong**	OI-3	A	-	1
S. lourencoi *	45–50	♂ 8–11 ♀ 7–8	4–5	7–8	44–45	10–14	8–9	17	♂ 1.9 ♀ 2.4	♂ **2.6** ♀ **2.95**	♂ **strong** ♀ **weak**	OI-1	**D**	**P4**	1
S. luridus	70–87	♂ 10 ♀ 8	4	12	75	60	9	17	♂ 2.7 ♀ -	♂ - ♀ -	♂ **strong** ♀ **weak**	OI-1	D	P3	0
S. margerisonae	40–50	♂ 9–13 ♀ 8–10	4	8	40	30	8–10	17	♂ 2.1 ♀ 2.2	♂ 2.5 ♀ -	♂ **strong** ♀ **moderate**	OI-1	D	P4	1
S. matthewi **sp. n.**	**60** (♀)	♂ - ♀ **4–5**	**6**	**8–9**	**59–71**	**20–31**	**6–7**	**17 (or 15)**	♂ - ♀ **2.78**	♂ - ♀ **2.54**	♂ - ♀ **weak**	OI-1	**D**	**P1**	**1**
S. novaki	44–49	♂ *8–9* ♀ *7–8*	4	11–13	70	60	8–9	18–19	♂ 3.6 ♀ 3.4–3.5	♂ 3.3 ♀ 3.2	♂ **strong** ♀ **moderate**	OI-3	A	P4	0
S. rufus ***	55.6–60.3	♂ 6–7 ♀ 5–6	**5**	**7**	**63**	**7**	6–8	17	♂ 2.5 ♀ 2.6	♂ **2.26** ♀ **2.05**	♂ **strong** ♀ **weak**	OI-1	D	**P1/P2**	0
S. songi	72 (♂)	♂ 7–**8** ♀ 6	**5**	**10**	**78**	**33**	7–8	17	♂ 2.3–2.4 ♀ -	♂ 3.0–3.1 ♀ -	♂ **strong** ♀ -	OI-1	D	P1	1
S. tibetanus *	50–57	♂ 4–7 ♀ 4–7	4–5	8–9	45–62	10–25	6–8	17	♂ 2.0 ♀ 2.0	♂ **2.65** ♀ **2.61**	♂ **strong** ♀ **weak**	OI-1	**D**	**P3**	0
S. vonwicki	52 (♀)	♂ - ♀ 5–6	4	11–13	65	10	7	17	♂ - ♀ 2.92	♂ - ♀ 3.0	♂ - ♀ **moderate**	OI-1	E	P2	1
S. wrzecionkoi	45–50	♂ **10–11** ♀ 8–9	4	8	60	30	9–11	18–20	♂ **2.52** ♀ 2.7	♂ - ♀ 2.6	♂ **strong** ♀ **moderate**	OI-1	D	P4	1

Table 2. Matrix of quantitative and qualitative diagnostic characters for *Scorpiops* recorded from Tibet (except for *S. hardwickii* and *S. petersii*). **Quantitative characters**: all sourced from Kovařík et al. (2020: 128–129: table 9), except for *Lv & Di (2022a), **Lv & Di (2022b), ***Lv & Di (2023), and the specimens examined in this paper. **Qualitative characters**: mostly limited to the ones that have been analyzed by Kovařík et al. (2020), since few Tibetan specimens are available for our examination. To clarify, OI is subjectively evaluated by the first author based on available illustrations and will not be particularly bolded, while MF-L, when bolded, is qualified by the same means. **Special fonts**: Data that are from Kovařík et al. (2020) but not exactly the same as those of the original Chinese descriptions are reddened; that are analyzed in this paper (either based on cited sources or specimens examined herein; calculated ratios are rounded values) are **bolded**; that are corrected from Kovařík et al. (2020) are *italicized*. **Abbreviations (besides those explained in Methods and text)**: MF-L, proximal lobe of pedipalp movable finger; F, fulcra. Fulcrum morphology is binary (0, absent; 1, present) and not subdivided into development degrees (e. g., reduced, moderate, strong).

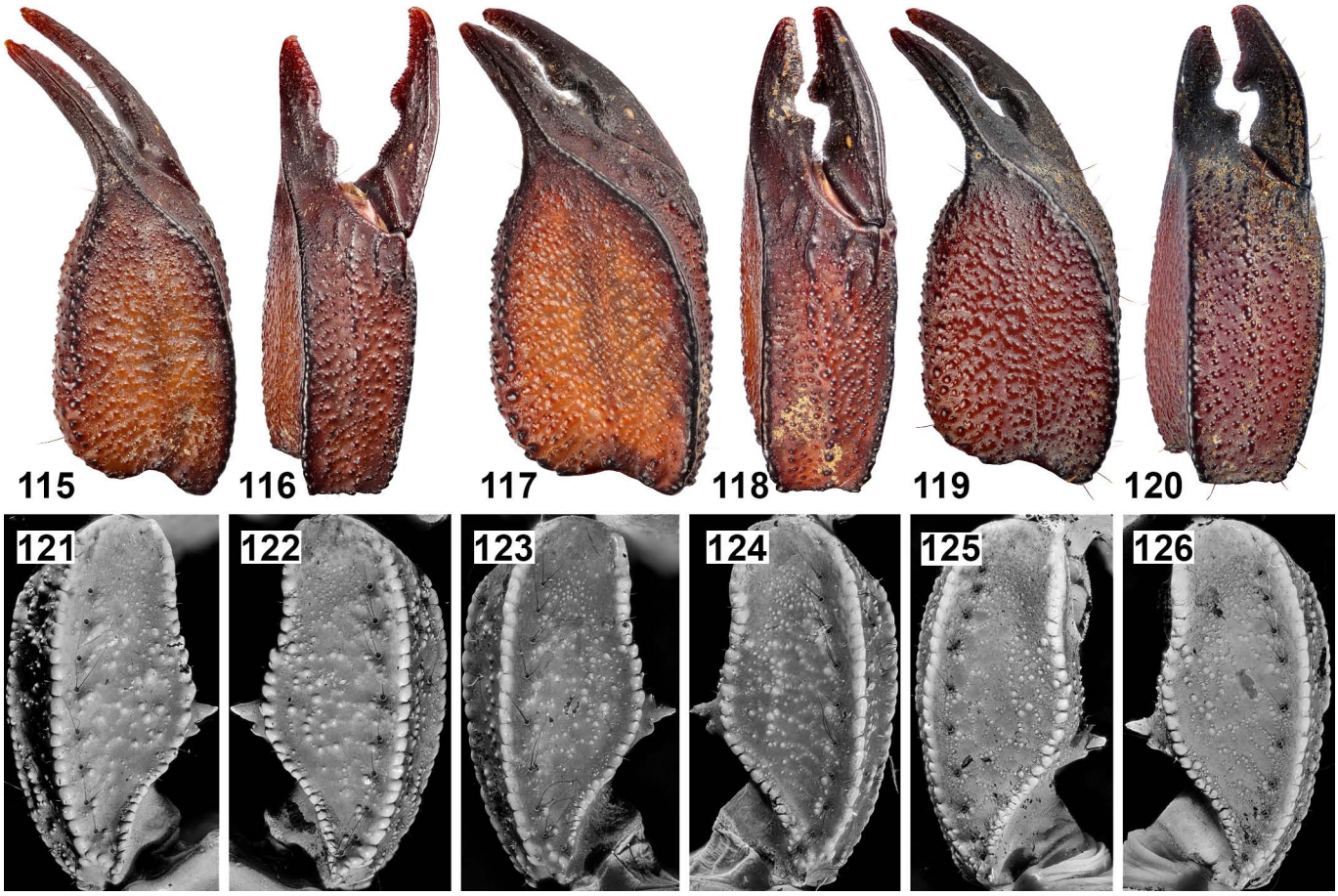

Figures 115–126: Comparison between *Scorpiops wrzecionkoi* and *S. margerisonae*. **Figures 115–120**. Right pedipalp chela in dorsal (115, 117, 119) and external (116, 118, 120) views, under white light: female (115–116) and male (117–118) *S. wrzecionkoi* and male *S. margerisonae* (119–120). **Figures 121–126**. Right (121, 123, 125) and left (122, 124, 126) pedipalp patella in ventral view, under UV light against black background: female (121–122) and male (123–124) *S. wrzecionkoi* and male *S. margerisonae* (125–126).

proportionally larger in comparison to the prosoma (Fig. 74 vs. Lv & Di, 2022b: fig. 35); **(2)** pedipalp chela more flattened and elongated (Figs. 86–87 vs. Lv & Di, 2022b: figs. 61–62); **(3)** pedipalp patella more elongated with distance between prodorsal and retrodorsal carinae narrower (Fig. 89 vs. Lv & Di, 2022b: fig. 54); **(4)** pedipalp femur more elongated with the distance between prodorsal and retrodorsal carinae not prominently increased distally, and retrodorsal carina not strongly undulate (Fig. 92 vs. Lv & Di, 2022b: fig. 53). From *S. lourencoi*, it differs as follows: **(1)** pedipalp chela proportionally larger in comparison to the prosoma (Fig. 74 vs. Lv & Di, 2022b: fig. 67); **(2)** pedipalp chela more flattened (Figs. 87 vs. Lv & Di, 2022b: figs. 94); **(3)** pedipalp chela not adorned by large, rounded granules (Figs. 86–87 vs. Lv & Di, 2022b: figs. 93); **(4)** pedipalp movable finger with stronger proximal lobe (Fig. 87 vs. Lv & Di, 2022b: figs. 94); **(5)** pedipalp patella more elongated with distance between prodorsal and retrodorsal carinae narrower (Fig. 89 vs. Lv & Di, 2022b: fig. 86); **(6)** pedipalp femur more elongated with the distance between prodorsal and retrodorsal carinae not prominently increased distally, and retrodorsal carina not strongly undulate (Fig. 92 vs. Lv & Di, 2022b: fig. 85); **(7)** different pectinal morphology with lower PTC (4 vs. 7–8 in females; Fig. 81 vs. Lv & Di, 2022b: fig. 77). With irrespective to the distribution range, within Tibet, *S. matthewi* **sp**. **n**. most resembles *S. ingens* from Lhasa by its overall features, including the relatively large and flattened pedipalp chela, proportionally long metasoma and elongated metasoma V (cf. Yin et al., 2015: fig. 3). However, a simple character allows the differentiation where *S. ingens* exhibits a different pectinal morphology (cf. Yin et al., 2015: fig. 8) with higher PTC (6–8 in females).

Within Xigazê, *S. matthewi* **sp**. **n**. appears to bear a much closer affinity with *S. rufus* in terms of the females, but several discovered distinctions raise reasonable doubts against considering them conspecific: **(1)** pedipalp chela proportionally larger in comparison to the prosoma (Fig. 74 vs. Lv & Di, 2023: fig. 3; ChL/CaL 1.79 in holotype *S. matthewi* **sp**. **n**. and 1.54 in paratype *S. rufus*; ChW/CaL 0.64 in holotype *S. matthewi* **sp**. **n**. and 0.6 in paratype *S. rufus*); **(2)** pedipalp chela more flattened (Fig. 87 vs. Lv & Di, 2023: fig. 32; *S. matthewi* **sp**. **n**. holotype Ch-D' = 3.72 mm, Ch-L/D' = 3.83, Ch-L/D = 3.04; *S. rufus* paratype Ch-L/D = 3.27, probably unstandardized); **(3)** external secondary carinae of chela composed of a longer, continuous and costate portion before deconstructing into discrete granules (Fig. 87 vs. Lv & Di,

No	Species (specimen code) [GenBank: cox1/16S]	1	2	3	4	5	6	7	8	9	10	11	12	13	14	15	16	17	
1	*S. anthracinus* (S652) [MW269416/MW250317]		0.000	0.002	0.142	0.144	n./a.	n./a.	n./a.	n./a.	n./a.	n./a.	0.147	0.137	0.122	0.134	0.146	0.164	p-distances cox1
2	*S. anthracinus* (S885) [MW269420/MW250320]	0.000		0.002	0.142	0.144	n./a.	n./a.	n./a.	n./a.	n./a.	n./a.	0.147	0.137	0.122	0.134	0.146	0.164	
3	*S. anthracinus* (S921) [MW269421/MW250321]	0.000	0.000		0.144	0.146	n./a.	n./a.	n./a.	n./a.	n./a.	n./a.	0.149	0.136	0.121	0.132	0.144	0.166	
4	*S. jendeki* (S2718) [PQ149985/PQ149976]	0.119	0.119	0.119		0.127	n./a.	n./a.	n./a.	n./a.	n./a.	n./a.	0.132	0.124	0.147	0.127	0.077	0.116	
5	*S. leptochirus* (S484) [MW269410/MW250310]	0.122	0.122	0.122	0.100		n./a.	n./a.	n./a.	n./a.	n./a.	n./a.	0.129	0.111	0.122	0.119	0.126	0.092	
6	*S. longimanus* (MZMU2010) [n.a./MW665151]	0.077	0.077	0.077	0.129	0.113		n./a.	n./a.	n./a.	n./a.	n./a.	n./a.	n./a.	n./a.	n./a.	n./a.	n./a.	
7	*S. longimanus* (MZMU2010A) [n.a./MW665152]	0.074	0.074	0.074	0.103	0.100	0.048		n./a.	n./a.	n./a.	n./a.	n./a.	n./a.	n./a.	n./a.	n./a.	n./a.	
8	*S. longimanus* (MZMU2010B) [n.a./MW665153]	0.074	0.074	0.074	0.103	0.100	0.048	0.000		n./a.	n./a.	n./a.	n./a.	n./a.	n./a.	n./a.	n./a.	n./a.	
9	*S. longimanus* (MZMU2042) [n.a./MZ057759]	0.077	0.077	0.077	0.106	0.096	0.048	0.006	0.006		n./a.	n./a.	n./a.	n./a.	n./a.	n./a.	n./a.	n./a.	
10	*S. longimanus* (MZMU2174) [n.a./MZ057760]	0.080	0.080	0.080	0.119	0.109	0.045	0.032	0.032	0.039		n./a.	n./a.	n./a.	n./a.	n./a.	n./a.	n./a.	
11	*S. longimanus* (MZMU2304A) [n.a./MZ057758]	0.055	0.055	0.055	0.113	0.106	0.039	0.032	0.032	0.039	0.035		n./a.	n./a.	n./a.	n./a.	n./a.	n./a.	
12	*S. montanus* (S853) [MW269419/MW250319]	0.161	0.161	0.161	0.138	0.138	0.135	0.129	0.129	0.129	0.132	0.141		0.142	0.146	0.146	0.136	0,134	
13	*S. tongtongi* (S2684) [PQ149983/PQ149974]	0.116	0.116	0.116	0.096	0.103	0.138	0.113	0.113	0.116	0.122	0.119	0.132		0.129	0.112	0.119	0.107	
14	*S. yangi* (S2717) [PQ149984/PQ149975]	0.100	0.100	0.100	0.125	0.113	0.077	0.077	0.077	0.074	0.077	0.080	0.132	0.122		0.109	0.142	0.131	
15	*S. deshpandei* **sp. n.** (S2720) [PQ149986/PQ14997	0.074	0.074	0.074	0.122	0.113	0.077	0.064	0.064	0.068	0.064	0.051	0,154	0.119	0.096		0.134	0.116	
16	*S. kovariki* **sp. n.** (S2721) [PQ149987/PQ149978]	0.122	0.122	0.122	0.019	0.106	0.132	0.109	0.109	0.113	0.122	0.116	0,141	0.103	0.125	0.125		0.111	
17	*S. matthewi* **sp. n.** (S2722) [PQ149988/PQ149979]	0.090	0.090	0.090	0.109	0.074	0.103	0.077	0.077	0.080	0.080	0.080	0,141	0.087	0.116	0.084	0.116		
		p-distances 16S																	

Table 3. Uncorrected pairwise genetic distances of cytochrome oxidase I (*coxI*) (above diagonal) and 16S rDNA (*16S*) (below diagonal) among selected *Scorpiops* species. Blue color indicates the intraspecific variability of *S. longimanus*. Green color indicates values of interspecies difference between *S. longimanus* and *S. deshpandei* **sp. n.** Red color indicates low values of interspecific differences between *S. jendeki* and *S. kovariki* **sp. n.**

2023: fig. 32); **(4)** interomedian carina of chela more straight and longer relative to ventromedian carina (conspicuously shorter and curved proximally in *S. rufus*), creating a smaller included angle when they are extended to the distal infinity (Fig. 88 vs. Lv & Di, 2023: fig. 33); **(5)** pedipalp patella more flattened with highly developed and costate retromedian carina (Fig. 90 vs. Lv & Di, 2023: fig. 25); **(6)** pedipalp femur more elongated with the distance between prodorsal and retrodorsal carinae not prominently increased distally, and retrodorsal carina not strongly undulate (Fig. 92 vs. Lv & Di, 2023: fig. 23; this is not influenced by the view angle, see other figures of the holotype and the compared species); **(7)** PTC lower (4–5 vs. 5–6 in females; Fig. 81 vs. Lv & Di, 2023: fig. 15); **(8)** pectinal fulcra present (vs. absent; Figs. 84 vs. Lv & Di, 2023: 325, fig. 15); **(9)** distal part of ventral surface outline of telson less convex when viewed laterally (Fig. 102 vs. Lv & Di, 2023: fig. 22; however, T-L/D contradicts this distinction). Another decisive character lies in the number of IAD on the pedipalp movable finger where numerous denticles (IAD) of unequal sizes are present along the MD series in all examined specimens (3 specimens, 6 fingers) of *S. matthewi* **sp. n.** yet such denticles are only paired with OAD in the male *S. rufus* (Figs. 95–96 vs. Lv & Di, 2023: fig. 30). While we acknowledge the incomparability between male and female specimens, sexual dimorphism is not known to exist in this regard. With reference to the observation in *S. tongtongi*, such intersexual discordance only presents in the series posterior to the proximal lobe (Tang, 2023: 8–9). Regrettably, no data was provided for the count of *S. rufus* in its original description. Geographically, both *S. lourencoi* and *S. matthewi* **sp. n.** are distributed on the south bank of Yarlung Tsangpo River, while *S. rufus* is on the north thereof (cf. Lv & Di, 2023: fig. 39). However, as no topotypes of the latter species were available for sequencing (and the coordinates for its type locality were also unknown), we cannot molecularly substantiate its validity against *S. rufus*. Nevertheless, the above listed differences justify it as a distinct species, particularly characters 2–5, 7–8 and number of IAD. The most salient character differentiating the two species is the "flatness" of pedipalp chela, where *S. matthewi* **sp. n.** exhibits a conspicuously more flattened chela with fairly narrow intraspecific variation in this regard. Since no specimens of *S. rufus* were available, the comparability and authenticity of the figures provided by Lv & Di (2023: figs. 28, 32) were confirmed by the chela photos of *S. atomatus* and *S. tibetanus* (for which specimens are available) given in Lv & Di (2022b), assuming their photographic setup and procedure remained consistent across papers. Specimens of *S. matthewi* **sp. n.** were also examined from different view angles to exclude the potential bias arising therefrom. Ultimately, the credibility of this diagnostic feature was affirmed by the inability to reproduce a similar visual effect of the chela in *S. matthewi* **sp. n.** compared to *S. rufus*.

The description for female *S. rufus* was founded upon four adults (Lv & Di, 2023: 325). The authors mentioned the following character variations: **(1)** coloration of female *S. rufus* (except for the pedipalps) lighter than that of males (Lv & Di, 2023: 328), being yellowish-brown; **(2)** PVTC: 6/7 (n = 1), 7/7 (n = 1), 7/8 (n = 1) and 8/8 (n = 1); **(3)** PTC: 5/5 (n = 1), 5/6 (n = 1), 6/5 (n = 1) and 6/6 (n = 1). Similarly, four adult females of *S. matthewi* **sp. n.** were documented with the following intraspecific variations: **(1)** coloration of legs consistently dark brown (vs. orangish brown to reddish brown; cf. Lv & Di, 2023: figs. 35–37); **(2)** PVTC: 6/7 (n = 1) and 7/7 (n = 3); **(3)** PTC: 4/4 (n = 3) and 5/5 (n = 1). The difference between the female PTC of two species is statistically significant (two-sample Mann-Whitney U test): p = 0.002108 (when treat all data as independent; n = 8 for each species) or 0.03599 (when take their means; n = 4 for each species). Crucially, this was based on a small sample size, hence the result remains referential. The variations for the two quantitative characters are incorporated into the diagnosis above.

Behavioral notes. The holotype of *S. matthewi* **sp. n.** was relatively ferocious and agitated, while also exhibiting a certain proclivity of avoiding threats by fleeing. No adoption of catalepsy was observed. In contrast, the female *S. margerisonae* was more docile and may remain motionless upon tactile stimulus introduced by finger. It did not promptly seek shelter after being exposed to light, as opposed to *S. matthewi* **sp. n.** However, a mere touch by the finger may not incite *S. matthewi* **sp. n.** to employ its pedipalp chela for pinching. Nevertheless, the scorpion displayed a defensive posture by opening these appendages.

Distribution. Known only from the type locality.

Scorpiops margerisonae Kovařík, 2000
(Figures 108, 111, 114, 119–120, 125–126)
http://zoobank.org/urn:lsid:zoobank.org:act:8CE10215-400C-4A55-BA9A-3854AF68BF55

Material examined. **CHINA**, ***Tibet Autonomous Region***, Lhasa City, Nyêmo (or Nimu) County, 29°19'00.7"N 90°18'43.8"E (29.31685629°N 90.31216129°E), 3698 m a. s. l., 20th July 2023, 1♂1juv.♀, leg. Tongtong, VT.

Remarks. *S. margerisonae* was originally described on the basis of a single adult male of unknown locality in Tibet (Kovařík, 2000: 189). This species was characterized by the presence of movable finger proximal lobe in male, a PVTC of 8–9, a PETC of 17 and a PTC of 12–13. A subsequent redescription was made by Di & Zhu (2010) where its female was reported for the first time. The materials examined by the authors were obtained from two prefecture-level cities in Tibet, Nyingchi (Nang County) and Shannan (Nêdong District), without precise coordinates. Most illustrations were hand drawn except for two colored photographs depicting the overall habitus in dorsal view (Di & Zhu, 2010: figs. 22–23). Qualitative characters are susceptible to inaccuracy if they were manually illustrated, which appears to be the case in their illustration for the male pectines. Referring to their quantitative characters, their new specimens were featured by a PVTC of 9–10, and a PTC of 9–12 (commonly 10–11) in males and 8–10 (commonly 8–9) in females. In the revision of Scorpiopidae by Kovařík et al. (2020: 129, table 9), those data from two sources were coalesced. Colored photographs for the pectine and chela of adult male *S. margerisonae* were provided (Kovařík et al., 2020: figs. 147, 227). According to their map (Kovařík et al., 2020: fig. 799), two records of *S. margerisonae* (labeled "47") appeared to be located between Lhasa and Shannan cities. The two new specimens examined in this study were collected from Nyêmo of Lhasa, which seems to be close to the left record on their map.

In the original description, Kovařík (2000: 189) considered *S. margerisonae* to be closest to *S. tibetanus*. During the current investigation, we checked all known Tibetan congeners and reckoned three species that share certain degrees of resemblance, *S. atomatus*, *S. tibetanus* and *S. wrzecionkoi*, all of which has a developed (regardless of the degree) proximal lobe in both sexes. *S. atomatus* is similar to *S. margerisonae* in the following characters: (1) PVTC 8–10; (2) PETC 17; (3) PTC 10–11 in males and 8–9 in females. Lv & Di (2022b: 212) considered *S. margerisonae* differs by a lower chela L/W ratio of 2.1–2.2 (more slender in females), while characterizing male and female *S. atomatus* as 2.3 and 2.5, respectively. In contrast, Kovařík et al. (2020: 129, table 9) documented male and female *S. margerisonae* as 2.2–2.3 and 2.2, respectively. This insinuates a weaker distinction between males of the two species in terms of their chela L/W ratio. The female *S. margerisonae* examined in this study possessed a noticeable proximal lobe which may imply maturity (Fig. 107), while its relatively small size suggests otherwise. No firm conclusion can be drawn as we are ignorant of the lobe possessed by an adult female *S. margerisonae*. If this female is a subadult, then both specimens quite resembled the adults of *S. atomatus* depicted in Lv & Di (2022b: figs. 1, 3). With reference to Kovařík et al. (2020) and Lv & Di (2022b), we discovered that the most prominent difference lies in the count of finger denticles where *S. atomatus* has 58–62 MD and 8–9 IAD, as opposed to the presence of 40 MD and 30 IAD in *S. margerisonae*; figures of movable finger dentition can be found in Kovařík et al. (2020: fig. 118) and Lv & Di (2022b: fig. 28). Our current examination also detected a discordance in pectinal morphology, where the pectinal teeth are shorter relative to the width of the pectinal lamellae in *S. atomatus* (cf. Lv & Di, 2022b: figs. 11, 13). The pectinal morphology of the adult male examined here accorded with the one depicted in Kovařík et al. (2020: fig. 147). Unlike *S. atomatus*, *S. tibetanus* can be more easily distinguished from *S. margerisonae* by its more rounded and robust pedipalp chela with strongly developed external secondary carinae (cf. Lv & Di, 2022b: figs. 58, 62) and a lower PTC (4–7 in both sexes), despite a more similar pectinal morphology in males.

Initially, considering the geographic proximity, the two specimens were presumed to be *S. wrzecionkoi*. According to the coordinates provided in the original description (29.20°N 90.58°E; Kovařík, 2020: 30), this species was described from Nagarzê County (near Sangjian) in Shannan City, based on two adult females and one juvenile. Our specimens were obtained from somewhere in Nyêmo, ca. 29.05 km northwest of the type locality of *S. wrzecionkoi*. Tang (2023: figs. 81–82) depicted a chela that was presumptively considered to belong to an adult male *S. wrzecionkoi*. This specimen, received as a gift from a researcher at the Chinese Academy of Science several years ago (around 2017) by the first author, was accompanied by an adult female. Unfortunately, no precise coordinates were provided for the two specimens, aside from the assertion that they were collected from Lhasa. Subsequent examination of the female specimen revealed a striking conformity with the original description for *S. wrzecionkoi*: (1) rectangular chela manus; (2) moderate proximal lobe on movable finger present; (3) pectines with 3 marginal and 4 middle lamellae; (4) PTC 8/9; (5) PVTC 9. Consequently, the male counterpart was identified. As a supplementary information, photos of those two dry specimens are included herein (Figs. 109–110, 112–113, 115–118, 121–124).

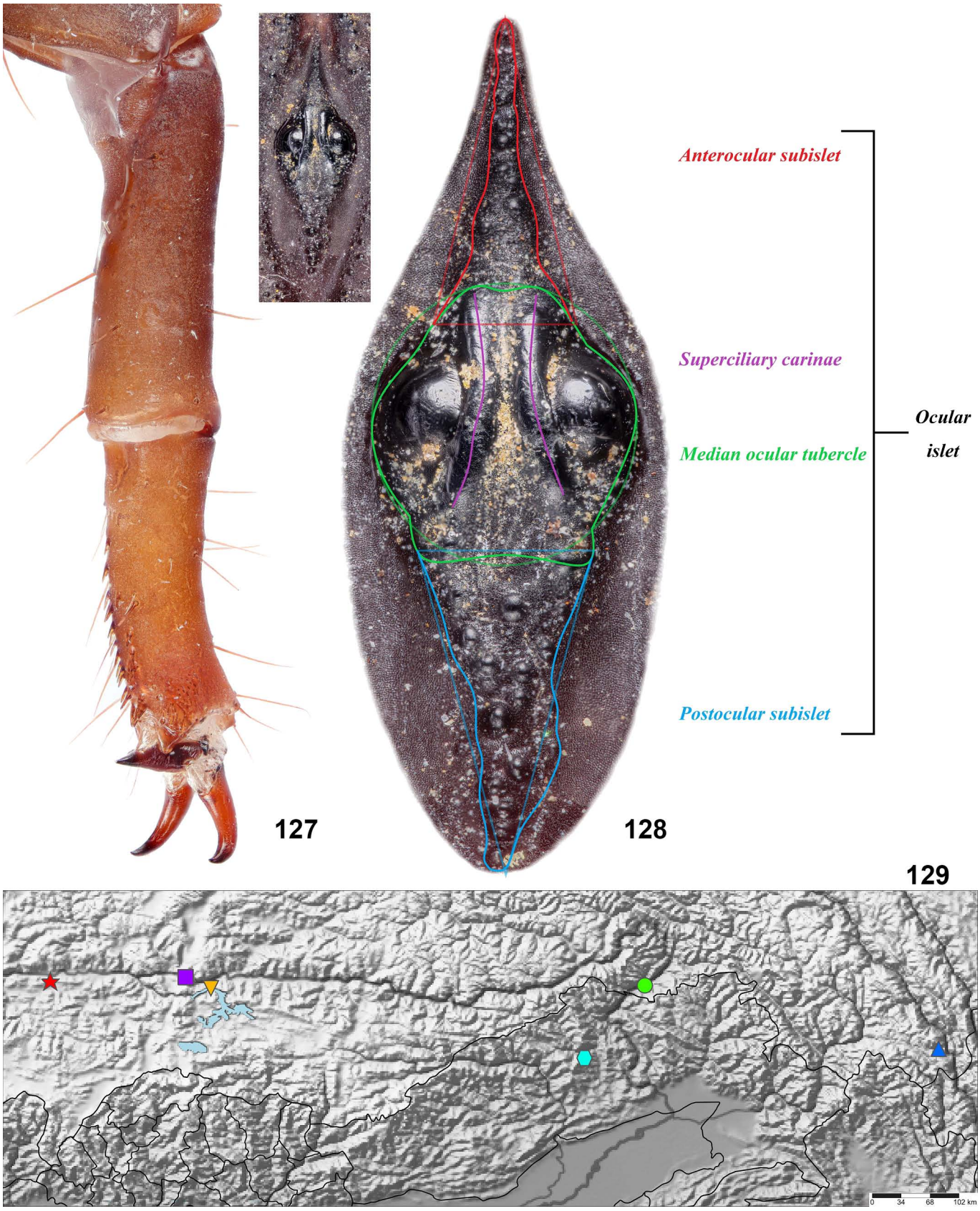

Figures 127–129. Regeneration of apotele on right 4th leg of *S. deshpandei* **sp**. **n**. holotype (127). Definition for the periocular morphology of median ocelli (OI, ocular islet) in Scorpiopidae with crudely fitted contour (50% transparence represents basic auxiliary geometry); exemplified by an adult female *Scorpiops grandjeani* (Vachon, 1974), in vivo (128). Map (129) showing the localities of *Scorpiops* spp.: *S. matthewi* **sp**. **n**. (★); *S. margerisonae* (■); *S. wrzecionkoi* (▼); *S. vonwicki* (⬢); *S. deshpandei* **sp**. **n**. (●); *S. kovariki* **sp**. **n**. (▲).

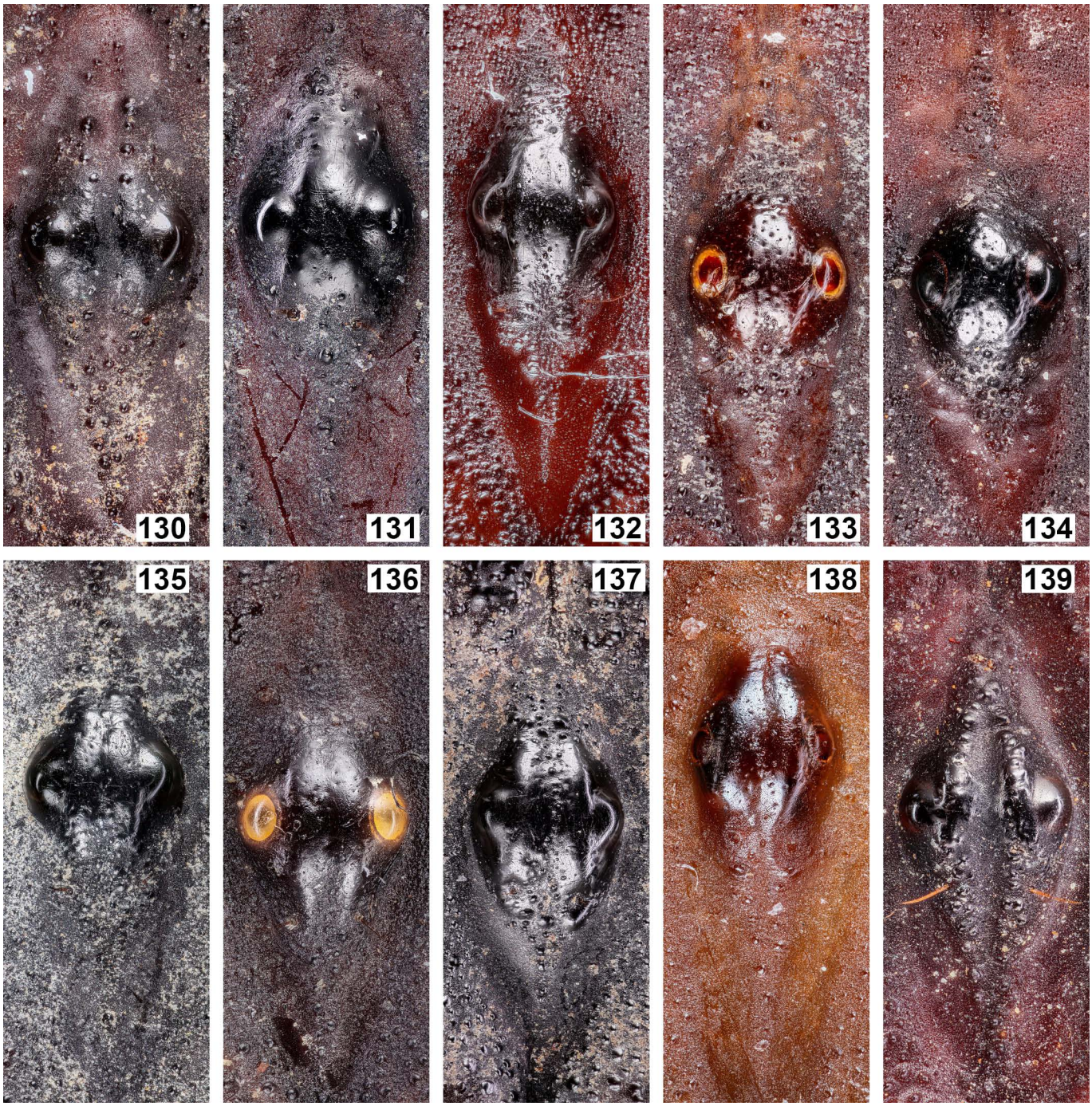

Figures 130–139. Comparison of median ocular islet between *S. deshpandei* **sp. n.** (130), *kovariki* **sp. n.** (131), *S. matthewi* **sp. n.** (132), *S. wrzecionkoi* (133–134; female and male), *S. margerisonae* (135; male), *S. atomatus* Qi et al., 2005 (136; female), *S. langxian* Qi et al., 2005 (137; female), *S. songi* Di & Qiao, 2022 (138; male) and *S. novaki* (Kovařík, 2005) (139; female); specimens have been preserved in ethanol prior to photography, except for *S. kovariki* **sp. n.** and dried specimens of *S. atomatus*, *S. songi* and *S. wrzecionkoi*. The distinctiveness of ocular tubercle is approximately conveyed by the area of reflection on the anterior and posterior surfaces. Larger area indicates a greater blockage in the light path induced by the tubercle, which is correlated with the "elevation" thereof. However, this also depends on the optical properties of the cuticular texture.

Since preserved specimens are susceptible to color alteration, our identification discarded the apparently yellowish brown tonality of *S. wrzecionkoi* specimens. When referring to the discrete quantitative characters, according to table 9 in Kovařík et al. (2020: 129), the two species share an overlapped PTC for both sexes (8–9 in female *S. wrzecionkoi*, with data of male based on the aforementioned specimen, 11/10), PVTC (9–11 in *S. wrzecionkoi*), and count of ID, OD and IAD (same for both species: 4, 8 and 30, respectively). However, *S. wrzecionkoi* has a higher count of MD (60). The pectinal morphology of both species is nearly indistinguishable. Nevertheless, the different chela profile

in our new specimens led to a negation of *S. wrzecionkoi* as its plausible identity. As observed in both the holotype female and the female examined herein, *S. wrzecionkoi* has a relatively elongated pedipalp chela. Although both male *S. margerisonae* and *S. wrzecionkoi* exhibit a quadrate chela profile, the fingers are proportionally shorter in the latter. In addition, the chela of *S. wrzecionkoi* appears to be somewhat more flattened. Consequently, considering both the geography and morphology, we identified our new specimens as *S. margerisonae*.

Tang (2023: figs. 86–88) also illustrated a chela of a presumed adult male *S. songi* from unknown locality. We continue to regard the specimen as that species and supplemented counts of denticles on its pedipalp movable finger in Table 2. Photos of the specimen can be found in the aforementioned supplementary PDF file available on ResearchGate.

Discussion

All species remain as hypotheses, as they are essentially inferred from the available data, yet their robustness varies depending on the species delimitation methods employed (Miralles et al., 2024). It is imperative to recognize the ongoing controversy surrounding contemporary methodologies for discriminating species boundaries, stemming from the absence of an objective and comprehensive paradigmatic framework universally adhered to by practitioners; however, some general guidelines for a taxonomy protocol have been recently proposed (e. g., Miralles et al., 2024). The species delineation, or the concept of species itself, mired in historical debate since the inception of taxonomy, remains a contentious issue. For invertebrates, traditional Linnaean taxonomy has prevalently relied on morphological characteristics. However, these superficial morphological traits may be influenced by natural phenomena such as homoplasy, stasis, or polymorphism, as well as artificial factors including sampling bias and mensurational inaccuracy. The uncertainty arisen from subjective assessments and the presence of various evolutionary mechanisms has been identified as a significant deficiency in morphology-based taxonomy. The advent of modern technology has witnessed the emergence of DNA taxonomy in the past two decades, leveraging DNA sequencing to delineate species boundaries or provide assistance in this regard as primary species hypotheses. Notably, DNA barcoding has gained popularity for its efficiency, facilitating rapid and direct inference of species boundaries from unknown samples based on a single gene fragment assumed to encapsulate all possible traits. This approach has been widely embraced, even leading to the emergence of "exclusive DNA-based taxonomy" (known as the "minimalist approach") where species are solely recognized and characterized by nucleotide sequences (which has been considered detrimental; Zamani et al., 2022). While DNA taxonomy is lauded for its ostensibly objective nature, deriving from fundamental components governing observable phenotypic traits, concerns persist regarding its inherent and inevitable subjectivity and inconsistency. Those defects are particularly pertinent regarding a manifold of molecular markers, different delimitation methodologies, and initial prior choices for the analysis parameters and empirical thresholds (Ahrens et al., 2021).

Although mitochondrial DNA (e.g., *coxI*) is favored for its simplicity and decreasing cost, it cannot be deemed infallible for inferring species boundaries, and certainly does not always (if at all) amount to the conclusive evidence for species recognition. Ahrens et al. (2021: 154) discussed how inferences based on a single mitochondrial gene are susceptible to errors due to extrachromosomal inheritance, resulting in a reduced rate of gene flow, limited recombination, incomplete lineage sorting, sex-biased dispersal, asymmetrical introgression, and/or *Wolbachia*-mediated genetic sweeps. As a result, divergence in mtDNA does not consistently signify speciation and may lead to an overestimation of true species diversity, particularly in the absence of corroborating evidence from nuclear genomic DNA and/or morphology. In addition, the distinctness of the barcode gap can be exaggerated by insufficient sampling. On the contrary, a low genetic distance does not necessarily imply conspecificity as the speciation can occur without genome-wide incompatibility (Miralles et al., 2024: 91). Similarly, young lineages are characterized by low genetic distances due to their recent speciation from a common ancestor and the limited time available for genetic differences to accumulate, but it does not preclude significant ecological or phenotypic divergence (Tarvin et al., 2017). Incomplete lineage sorting (ILS) is known to display in young groups (Zamani et al., 2022: 6), whereas ILS itself may result in misleading or uninformative genealogical histories of individual gene loci about the relationships among species or populations (Maddison & Knowle, 2006), such as the apparently shallow genetic divergence (Pereira & Schrago, 2018) in certain genomic regions due to the stochastic retention of ancestral genetic variation (polymorphism), where the alleles coalesced more recently than the actual species divergence time. One of our new species, *S. kovariki* **sp**. **n**., is characterized by its small p-distance from its close relative, *S. jendeki*. *S. jendeki* is a widespread species putatively with a large effective population size which may increase the occurrence likelihood of ILS. This can lead to situations where genetically close congeners, which may have diverged phenotypically due to different selection pressures, are found in nearby regions. *S. jendeki* displays a stable combination of morphological features where the observed phenotypes in *S. kovariki* **sp**. **n**. are excluded. Phenotypic traits can evolve relatively quickly due to natural selection, even when genetic divergence is incomplete. This motivated us to prioritize the morphological distinction over the molecular similarity, hereby justifying the validity of our new species. Chela morphology is hypervariable among *Scorpiops* species, leading to the divergence in their ratiometrics and trichobothrial position diagnostic at species level, but the precise selective pressure that drives the evolution of costate and granular carinae is yet unknown.

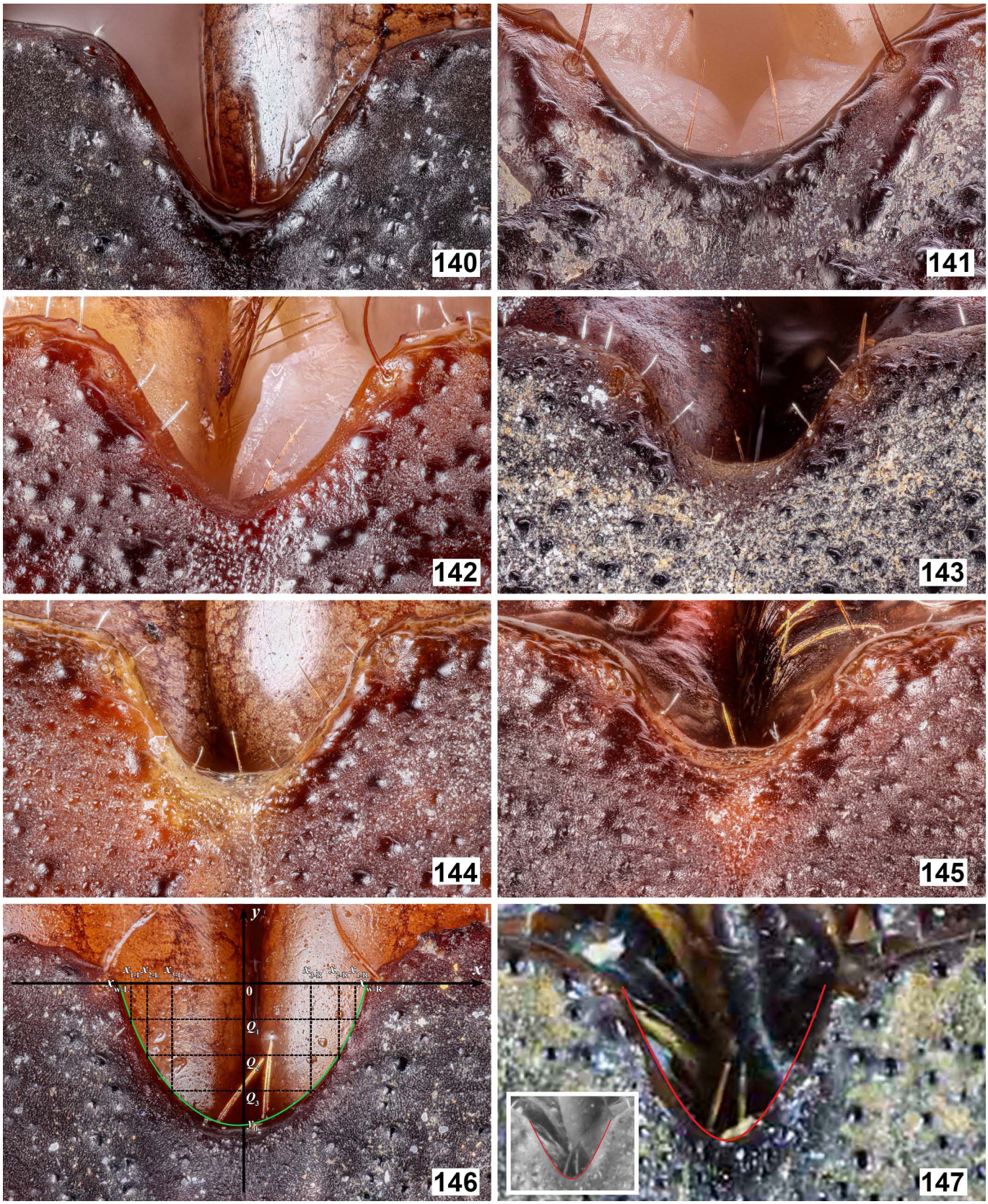

Figures 140–147. Comparison of anteromedian notch between *S. deshpandei* **sp**. **n**. (140), *S. kovariki* **sp**. **n**. (141), *S. matthewi* **sp**. **n**. (142), *S. margerisonae* (143), *S. wrzecionkoi* (144–145; female and male), *S. lowei* Tang, 2022 (146; paratype male) and *S. kubani* (Kovařík, 2004) (147; paratype male, and a UV counterpart; photo courtesy of F. Kovařík); specimens have been preserved in ethanol prior to photography, except for *S. kovariki* **sp**. **n**. and dried specimens of *S. wrzecionkoi*. Green and red curves in Figs. 146–147 are fitted to the outline. Fig. 146 illustrates a feasible geometric analysis method: two trichobothria serve as the landmarks that define the *x*-axis, with the width of the notch calculated by $|x_{w\text{-}L} - x_{w\text{-}R}|$ and its depth by $|0 - y_d|$ where *y*-axis is the median axis of the carapace. As a crude example, the profile of the notch can either be analyzed by the function of a curve fitted onto it, or by partitioning the depth into several quantiles, thereby quantifying the relative distances at each quantile. Here, the depth is severed by quartiles (Q_1, Q_2, Q_3), each corresponding to two *x* values (left and right) that can be further analyzed. Indeed, in the sense of calculus, as the number of quantiles increases, the precision of the notch geometry also tends to rise.

In any case, it is crucial to critically evaluate our results, despite ostensibly employing an integrative approach based on both morphological and molecular evidence in an attempt to support the identification of two of our new species. However, integrative taxonomy necessitates technologies (e.g., PCR) commonly inaccessible to independent amateur taxonomists (e.g., the first author), prompting them to establish collaborations with institutional researchers (e.g., the fourth author). Despite taxonomy representing the cornerstone of all biological fields (Braby et al., 2024), it remains undervalued and frequently underfunded (Löbl et al., 2023). This lack of funding forces researchers to maximize cost efficiency, which can delay analyses entailing only a handful of species, thereby decreasing the efficiency of taxonomic description. Such delays are detrimental in the current global context, where humanity faces an Anthropocene mass extinction of biodiversity.

Taxonomy, the discipline dedicated to delineating, circumscribing and categorizing hypothetical lineages of organisms, underpins all fields in the biological sciences (including conservation biology, primary industry, medicine, and public health). As May (1990) aptly stated, "*Without taxonomy to give shape to the bricks*, *and systematics to tell us how to put them together*, *the house of biological science is a meaningless jumble.*" The studies of physiology, ecology and evolutionary biology would be superficial and meaningless if species are not delimited and named to facilitate comparisons (even if they remain as Operational Taxonomic Units), thence a holistic and comprehensive epistemological framework that provides broader and deeper insights cannot be achieved. Although often being criticized for its accuracy and authenticity, morphology remains the most accessible and interpretable avenue for the end-users of taxonomy in the current era where identification (or integrative) based on DNA (partial or whole-genome) is not readily feasible for the general public. The preceding identification of *Scorpiops* species has relied heavily on a few quantitative morphological characters. On the contrary, the current study intends to highlight the diagnostic utility of several qualitative characters. Previously, the discovery of a new species from Yunnan (*S. tongtongi*) prompted the first author to conduct a preliminary review on its congeners within that province (Tang, 2022b). The scarcity of specimen (1 adult female) forced the author to ferret out additional characters, such that the validity of that species can be supported. In fact, the author swiftly realized that it was a new species upon observing the shape of its median ocular tubercle – a feature which has been seemingly overlooked in the past. Additionally, two other qualitative characters were brought to attention: the spiniform apophysis on pedipalp patella (strong or weak, seemingly correlated with the slenderness of pedipalp) and the formation of carinae on pedipalp chela (costate or granular). In Tang (2022c), one of the diagnostic features of *S. lowei* Tang, 2022 that distinguishes it from *S. kubani* (Kovařík, 2004) was proposed as the shape of the anteromedian notch of carapace, which is also described and illustrated in the current study (Figs. 140–147). This character, while appearing stable in some species (cf. Tang, 2022c: figs. 12–18, 23, 25), may be variable in others (i.e., phenotypic plasticity; e.g., Figs. 144–145). Meritoriously, some meticulous authors have also noticed the diagnostic potential of some unobtrusive interspecific variations of this structure (Mirza et al., 2014: 146; Zambre et al., 2014: 401–402). However, their focus was centered upon the presence/absence of the marginal ridge along this edge. Indeed, as evidently depicted in Figs. 140–147, such edge, formed by fused elongated granules, can be absent in some species. Later, Sulakhe et al. (2021: 41) incorporated the depth of the anteromedian notch as a diagnostic feature in their dichotomous keys. A further review on the Chinese *Scorpiops* species by Tang (2023) has built a foundation for our understanding and methodology targeting the study of this genus, upon which the current study is grounded. Quantitative characters (numerical or ratiometric) are indeed more objective in practice. However, due to their biased nature acquired during the process of enumeration and measurement, several quantitative characters may occasionally prove to be more convenient and less misleading. Coincidentally, one of our new species, *S. kovariki* **sp**. **n**., could only be distinguished by one quantitative character from *S. jendeki*. It is noteworthy that all qualitative characters are theoretically quantifiable, but the process can be intricate, and the results may be less interpretable, straightforward, or intuitive. Accompanying the assertions with photographic evidences improves the conceivability. As a result, in a steadfast endeavor to steer clear of the fallacy of Ockham's Broom, visual proofs were supplemented for the erstwhile taxonomic papers of the first author.

The diversity of *Scorpiops* species in China is undeniably astounding. Hitherto, 33 species are already described and/or recorded from this country, including the three new species described in the present paper, even if one were to discount the two non-endemic species with dubious records (*S. hardwickii* and *S. petersii*). During the present investigation, we noticed that a neglected species, *S. vonwicki*, which was described based on a single female from Arunachal Pradesh in India, was elevated to the species rank from a subspecies of *S. petersii* (Kovařík, 2020: 26–30). However, this region is politically contested due to the complex history between China and India, both claiming it as their own territory. While our interest remains on nature science and never politics, in line with the considerations for *S. asthenurus*, *S. kamengensis* and *S. leptochirus* Pocock, 1893 as per Tang (2023: 48), we have thus incorporated it into the Chinese scorpiofauna of this genus as above (an updated checklist will be published in the future). According to Kovařík et al. (2020: fig. 799), Sulakhe et al. (2021), Lourenço & Ythier (2022) and Nawanetiwong et al. (2024), the distribution of *Scorpiops* species is documented as follows: 30 species (with 2 known only from the aforementioned politically disputed area) from India, 23 from Thailand, 8 from Vietnam, 7 from Laos, Myanmar, and Pakistan respectively, 4 from Nepal, 2 from Afghanistan, Bangladesh, and Bhutan respectively, and 1 from Malaysia. This renders China to be the top country in *Scorpiops* diversity (34 spp.).

Indeed, the geographical distribution of *Scorpiops* species in China presents an intriguing pattern. Currently, with irrespective to *S. hardwickii* and *S. petersii*, 21/34 species are from Tibet, while 10/34 are from Yunnan. The species found in those two regions show a certain level of micro-endemism, highly diversified within a small area, while also displaying a morphological conservativism to some extent with limited degrees of interspecific differences. One new species hereby described, *S. matthewi* **sp**. **n**., adds another layer of regional diversification of this genus within Xigazê (accompanied by *S. lourencoi* and *S. rufus*). In fact, such phenomenon has been observed in previous studies, attested by the presence of nine species clustered within a small area in the northern Western Ghats of India (Sulakhe et al., 2021: fig. 153). The remaining three species, including one *nomen nudum* ("*S. jingshanensis*"), are scattered across Xinjiang (*S. taxkorgan*), Chongqing (*S. zhui*) and Hubei ("*S. jingshanensis*") provinces. While the populations in Tibet and Yunnan are in close proximity with the foreign species, those three species, particularly *S. zhui* and "*S. jingshanensis*", are noteworthy for their isolated occurrence. The substantial geographical distance between these two species and any other congeners suggests that there are likely more new species awaiting discovery from the areas in between.

Acknowledgements

We would like to thank Yong Yang (杨勇) for his assistance in the international delivery of DNA samples. Appreciation goes to Dr. Graeme Lowe and two anonymous reviewers for their comments on the manuscript.

References

AHRENS, D., S. T. AHYONG, A. BALLERIO, M. V. L. BARCLAY, J. EBERLE, M. ESPELAND, B. A. HUBER, X. MENGUAL, T. L. PACHECO, R. S. PETERS, B. RULIK, F. VAZ-DE-MELLO, T. WESENER & F.-T. KRELL. 2021. Is it time to describe new species without diagnoses? A comment on Sharkey et al. (2021). *Zootaxa*, 5027(2): 151–159.

BRABY, M. F., Y.-F. HSU & G. LAMAS. 2024. How to describe a new species in zoology and avoid mistakes. *Zoological Journal of the Linnean Society*, 20: 1–16.

DI, Z.-Y. & S. QIAO. 2020. *Euscorpiops lii* sp. nov. and a key of the genus *Euscorpiops* Vachon, 1980 (Scorpiones, Scorpiopidae) from China. *ZooKeys*, 968: 71–83.

DI, Z.-Y. & M.-S. ZHU. 2010. Redescription of *Scorpiops margerisonae* Kovařík, 2000, with the first record of its female, from China (Xizang) (Scorpiones: Euscorpiidae: Scorpiopinae). *Euscorpius*, 104: 1–9.

FOLMER, O., M. BLACK, W. HOEH, R. LUTZ & R. VRIJENHOEK. 1994. DNA primers for amplification of mitochondrial cytochrome c oxidase subunit I from diverse metazoan invertebrates. *Molecular Marine Biology and Biotechnology*, 3: 294–299.

GANTENBEIN, B., V. FET, C.R. LARGIADÈR & A. SCHOLL. 1999. First DNA phylogeny of *Euscorpius* Thorell, 1876 (Scorpiones, Euscorpiidae) and its bearing on taxonomy and biogeography of this genus. *Biogeographica*, 75: 49–65.

KOVAŘÍK, F. 2000. Revision of family Scorpiopidae (Scorpiones), with descriptions of six new species. *Acta Societatis Zoologicae Bohemicae*, 64: 153–201.

KOVAŘÍK, F. 2005. Three new species of the genera *Euscorpiops* Vachon, 1980 and *Scorpiops* Peters, 1861 from Asia (Scorpiones: Euscorpiidae, Scorpiopinae). *Euscorpius*, 27: 1–10.

KOVAŘÍK, F. 2020. Nine new species of *Scorpiop*s Peters, 1861 (Scorpiones: Scorpiopidae) from China, India, Nepal, and Pakistan. *Euscorpius*, 302: 1–40.

KOVAŘÍK, F., G. LOWE, M. STOCKMANN & F. ŠŤÁHLAVSKÝ. 2020. Revision of genus-group taxa in the family Scorpiopidae Kraepelin, 1905, with description of 15 new species (Arachnida: Scorpiones). *Euscorpius*, 325: 1–142.

LÖBL, I., B. KLAUSNITZER, M. HARTMANN & F.-T. KRELL. 2023. The silent extinction of species and taxonomists-an appeal to science policymakers and legislators. *Diversity*, 15(1053): 1–17.

LOURENÇO, W. R. & E. YTHIER. 2022. A new species of the genus *Scorpiops* Peters, 1861, subgenus *Euscorpiops* Vachon, 1980 from Laos (Scorpiones: Scorpiopidae). *Faunitaxys*, 10(27): 1–9.

LV, H.-Y & Z.-Y DI. 2022a. The first record of *Scorpiops bhutanensis* Tikader & Bastawade, 1983 from China, with the first report of its female (Scorpiones: Scorpiopidae). *Euscorpius*, 358: 1–8.

LV, H.-Y & Z.-Y DI. 2022b. *Scorpiops lourencoi* sp. nov., the revalidation of *Scorpiops atomatus* Qi, Zhu & Lourenço, 2005, and the redescription of *Scorpiops tibetanus* Hirst, 1911 (Scorpiones, Scorpiopidae) from China. *ZooKeys*, 1132: 189–214.

LV, H.-Y & Z.-Y DI. 2023. A new species of the genus *Scorpiops* Peters, 1861 from Xizang, China (Scorpiones: Scorpiopidae). *Arthropoda Selecta*, 32(3): 323–332.

MADDISON, W. P. & L. L. KNOWLE. 2006 Inferring phylogeny despite incomplete lineage sorting. *Systematic Biology*, 55(l): 21–3.

MALSAWMDAWNGLIANA, F., M. VABEIRYUREILAI, V. SIAMMAWII, L. MUANSANGA , G. Z. HMAR, H. DECEMSON & H. T. LALREMSANGA. 2022. On the occurrence of *Scorpiops longimanus* (Pocock, 1893) (Arachnida: Scorpiopidae) in Mizoram, northeast India. *Taprobanica*, 11(1): 4–11.

MAY, R. M. 1990. Taxonomy as destiny. *Nature*, 347: 129–130. https://doi.org/10.1038/347129a0

MIRALLES, A., N. PUILLANDRE & M. VENCES. 2024. DNA barcoding in species delimitation: from genetic distances to integrative taxonomy. *In*: DeSalle, R. (ed.). *DNA barcoding: methods and protocols* (Methods in Molecular Biology, vol. 2744). New York: Springer-Verlag, 576 pp. https://doi.org/10.1007/978-1-0716-3581-0_4

MIRZA, Z. A., R. J. SANAP & R. UPADHYE. 2014. A new species of scorpion of the genus *Neoscorpiops* Vachon, 1980 (Scorpiones: Euscorpiidae) from India. *Comptes Rendus Biologies*, 337 (2): 143–149.

NAWANETIWONG, W., O. KOŠULIČ, N. WARRIT, W. R. LOURENÇO & E. YTHIER. 2024. A new species of the genus *Scorpiops* Peters, 1861, subgenus *Euscorpiops* Vachon, 1980 from Thailand (Scorpiones, Scorpiopidae). *ZooKeys*, 1193: 161–170.

PEREIRA, A. G. & C. G. SCHRAGO. 2018 Incomplete lineage sorting impacts the inference of macroevolutionary regimes from molecular phylogenies when concatenation is employed: an analysis based on Cetacea. *Ecology and Evolution*, 8(14): 6965–6971.

SIMON, C., F. FRATI, A. BECKENBACH, B. CRESPI, H. LIU & P. FLOOK. 1994. Evolution, weighting, and phylogenetic utility of mitochondrial gene sequences and a compilation of conserved polymerase chain reaction primers. *Annals of the Entomological Society of America*, 87: 651–701.

SULAKHE, S., S. DESHPANDE, N. DANDEKAR, A. PADHYE & D. BASTAWADE. 2021. Four new lithophilic species of *Scorpiops* Peters, 1861 (Scorpiones: Scorpiopidae) from peninsular India. *Euscorpius*, 337: 1–49.

ŠTUNDLOVÁ, J., J. ŠMÍD, P. NGUYEN & F. ŠŤÁHLAVSKÝ. 2019. Cryptic diversity and dynamic chromosome evolution in Alpine scorpions (Euscorpiidae: *Euscorpius*). *Molecular Phylogenetics and Evolution*, 134: 152–163.

ŠŤÁHLAVSKÝ F., F. KOVAŘÍK, M. STOCKMANN & V. OPATOVÁ. 2021. Karyotype evolution and preliminary molecular assessment of genera in the family Scorpiopidae (Arachnida: Scorpiones). *Zoology*, 144: 125882.

TAMURA, K., G. STECHER & S. KUMAR. 2021. MEGA11: Molecular Evolutionary Genetics Analysis version 11. *Molecular Biology and Evolution*, 38: 3022–3027.

TANG, V. 2022a. A standardized list of scorpion names in Chinese, with an etymological approach. *Euscorpius*, 350: 1–91.

TANG, V. 2022b. A new species of genus *Scorpiops* Peters, 1861 from Yunnan Province, China, with a preliminary review on its congeners in Yunnan (Scorpiones: Scorpiopidae). *Euscorpius*, 360: 1–45.

TANG, V. 2022c. Reanalysis of the Yunnan population of *Scorpiops kubani* (Kovařík, 2004) with a description of a new species, *Scorpiops lowei* sp. n. (Scorpiones: Scorpiopidae). *Euscorpius*, 361: 1–22.

TANG, V. 2023. Description of the adult male *Scorpiops tongtongi* Tang, 2022, with further comments on the genus *Scorpiops* Peters, 1861 in China (Scorpiones: Scorpiopidae). *Euscorpius*, 377: 1–52.

TANG, V., Z.-B. LIU, M. R. GRAHAM, V. FET, F. KOVAŘÍK & F. ŠŤÁHLAVSKÝ. 2024b. Revision of the genus *Olivierus* in Xinjiang, China, with comments on *Mesobuthus thersites* (Scorpiones: Buthidae). *Euscorpius*, 383: 1–58.

TARVIN, R. D., E. A. POWELL, J. C. SANTOS, S. R. RON & D. C. CANNATELLA. 2017. The birth of aposematism: high phenotypic divergence and low genetic diversity in a young clade of poison frogs. *Molecular Phylogenetics and Evolution*, 109: 283–295.

WÜSTER, W., S. A. THOMSON, M. O'SHEA & H. KAISER. 2021. Confronting taxonomic vandalism in biology: conscientious community self-organization can preserve nomenclatural stability. *Biological Journal of the Linnean Society*, 133: 645–670.

YIN, S.-J., Y.-F. ZHANG, Z.-H. PAN, S.-B. LI & Z.-Y. DI. 2015b. *Scorpiops ingens* sp. n. and an updated key to the *Scorpiops* from China (Scorpiones, Euscorpiidae, Scorpiopinae). *ZooKeys*, 495: 53–61.

YTHIER, E. 2024. A new high-elevation scorpion species of the genus *Hottentotta* Birula, 1908 (Scorpiones: Buthidae) from Tibet, China. *Arachnides*, 114: 1–10.

ZAMANI, A., D. D. POS, Z. F. FRIC, A. B. ORFINGER, M. D. SCHERZ, A. S. BARTOŇOVÁ & H. F. GANTE. 2022. The future of zoological taxonomy is integrative, not minimalist. *Systematics and Biodiversity*, 20(1): 1–14.

ZAMBRE, A., R. V. SANAP & Z. A. MIRZA. 2014. A new high-elevation scorpion species of the genus *Scorpiops* Peters, 1861 (Scorpiones: Euscorpiidae: Scorpiopinae) from the Himalayas, India. *Comptes Rendus Biologies*, 337: 399–404.